Fraunhofer Institut
Techno- und
Wirtschaftsmathematik

J. Orlik

Homogenization for contact problems with periodically rough surfaces

Berichte des Fraunhofer ITWM, Nr. 59 (2004)

ISSN 1434-9973

Bericht 59 (2004)

Die Veröffentlichungen in der Berichtsreihe des Fraunhofer ITWM können bezogen werden über:

Fraunhofer-Institut für Techno- und
Wirtschaftsmathematik ITWM
Gottlieb-Daimler-Straße, Geb. 49

67663 Kaiserslautern
Germany

Telefon: +49 (0) 6 31/2 05-32 42
Telefax: +49 (0) 6 31/2 05-41 39
E-Mail: info@itwm.fraunhofer.de
Internet: www.itwm.fraunhofer.de

Vorwort

Das Tätigkeitsfeld des Fraunhofer Instituts für Techno- und Wirtschaftsmathematik ITWM umfasst anwendungsnahe Grundlagenforschung, angewandte Forschung sowie Beratung und kundenspezifische Lösungen auf allen Gebieten, die für Techno- und Wirtschaftsmathematik bedeutsam sind.

In der Reihe »Berichte des Fraunhofer ITWM« soll die Arbeit des Instituts kontinuierlich einer interessierten Öffentlichkeit in Industrie, Wirtschaft und Wissenschaft vorgestellt werden. Durch die enge Verzahnung mit dem Fachbereich Mathematik der Universität Kaiserslautern sowie durch zahlreiche Kooperationen mit internationalen Institutionen und Hochschulen in den Bereichen Ausbildung und Forschung ist ein großes Potenzial für Forschungsberichte vorhanden. In die Berichtreihe sollen sowohl hervorragende Diplom- und Projektarbeiten und Dissertationen als auch Forschungsberichte der Institutsmitarbeiter und Institutsgäste zu aktuellen Fragen der Techno- und Wirtschaftsmathematik aufgenommen werden.

Darüberhinaus bietet die Reihe ein Forum für die Berichterstattung über die zahlreichen Kooperationsprojekte des Instituts mit Partnern aus Industrie und Wirtschaft.

Berichterstattung heißt hier Dokumentation darüber, wie aktuelle Ergebnisse aus mathematischer Forschungs- und Entwicklungsarbeit in industrielle Anwendungen und Softwareprodukte transferiert werden, und wie umgekehrt Probleme der Praxis neue interessante mathematische Fragestellungen generieren.

Prof. Dr. Dieter Prätzel-Wolters
Institutsleiter

Kaiserslautern, im Juni 2001

HOMOGENIZATION FOR CONTACT PROBLEMS WITH PERIODICALLY ROUGH SURFACES

Julia Orlik
Fraunhofer Institut Techno- und Wirtschaftsmathematik
Kaiserslautern, Germany

Abstract

We consider the contact of two elastic bodies with rough surfaces at the interface. The size of the micro-peaks and -valleys is very small compared with the macrosize of the bodies' domains. This makes the direct application of the FEM for the calculation of the contact problem prohibitively costly. A method is developed that allows deriving a macrocontact condition on the interface. The method involves the two-scale asymptotic homogenization procedure that takes into account the microgeometry of the interface layer and the stiffnesses of materials of both domains. The macrocontact condition can then be used in a FEM model for the contact problem on the macrolevel. The averaged contact stiffness obtained allows the replacement of the interface layer in the macromodel by the macrocontact condition.

1 INTRODUCTION

Contact problems of elastic bodies appear in many applications of solid mechanics. The macrocontact conditions are known to be rather influenced by the microroughness of the contacting surfaces. In Sec.2, we first use the standard penalty method and a certain smoothing procedure for the friction term to approximate the variational inequality of the contact problem by a variational equation. Then, we give mechanical interpretation of the approximated contact conditions for their possible future application in the commercial FE-software. We introduce a small parameter ε, which is related on the period of the microroughness on the contacting interface. Then, we demonstrate the existence of the solution in contact domains with some microroughness on the interface and show that the solution is bounded uniformly in ε. Since our contact problem has two different size scales on the micro- and macrolevels, it is very difficult to perform its direct numerical solution. So we intend in Sec.3 to reduce the problem to a single-scale problem through the

Keywords: asymptotic homogenization, contact problems

two-scale homogenization technique. Two lemmas of Yosifian (1997,2001) about convergence of the surface integrals over nonlinear functions of the weak convergent arguments are used as a main instrument in this section. Lemma 31 and Proposition 32 yield the main result of this section. The main conclusion in the mechanical sense is that even starting with the frictionless contact micro-problem with a rough interface, we end up with the macro-problem containing friction. We also propose a two-scale algorithm for the solution of the contact problem in this section and give a numerical example for some special simple microgeometry in the last section.

2 Signorini's Problem with Friction

2.1 Statement of the Microcontact problem

We consider two contacting domains, D^ε, $\Omega^\varepsilon \subset \mathbb{R}^n$, as schematically shown in Fig. 1. A part of the boundary of D^ε is assumed to have a pattern represented by peaks with summits arranged periodically with period εT, where ε is a small parameter. The domain Ω^ε is in contact with D^ε at the summits. We assume that D^ε and Ω^ε are Lipschitz domains in the n-dimensional Euclidean space; in applications $n = 2$ or 3 but our reasoning and relations obtained below will be valid for any n. We introduce also fixed domains $\Omega \subset \Omega^\varepsilon$ and $D \subset D^\varepsilon$ such that $(\Omega^\varepsilon \cup D^\varepsilon) \setminus (\Omega \cup D) \subset \Pi^\varepsilon$, where Π^ε is the thin layer containing the peaks of D^ε (Fig. 1); the measure of $(\Omega^\varepsilon \cup D^\varepsilon) \setminus (\Omega \cup D)$ tends to zero as $\varepsilon \to 0$. Let $x = (x_1, \dots, x_n)$ and $\hat{x} = (x_2, \dots, x_n)$ be the coordinates of a point in $\mathbb{R}^n$ and those of a point at the hyperplane $x_1 = 0$. We denote by Y an expanded periodicity cube, $Y = \{\xi \in \mathbb{R}^n : 0 < \xi_j < Y_0,\ j = 1, \dots, n\}$, and by Y_1 its infinite extension in the ξ_1 direction, $Y_1 = \{\xi \in \mathbb{R}^n : 0 < \xi_j < Y_0,\ j = 2, \dots, n\}$, and introduce local coordinates that are related to x by $x = \varepsilon\xi$. Additionally, we denote by T the cross section of the periodicity cell by a hyperplane $\xi_1 = \text{const}$, i.e., $T = \{\xi \in Y : \xi_1 = \text{const}\}$. Furthermore, the microcontact surfaces will be defined by $S_C^{A^\varepsilon} = \{x \in \mathbb{R}^n : \hat{x} \in \text{Proj}_{\{x_1=0\}} S_0^A,\ x_1 = \Phi^A(\hat{x}) + \varepsilon F^A(\hat{x}, \frac{\hat{x}}{\varepsilon})\}$, where $S_0^A = \{x : x_1 = \Phi^A(\hat{x})\}$ is the macrocontact surface, $A := \{\Omega, D\}$, Φ^A and F^A are Lipschitz functions describing parametrically the macro- and micro-contact surface belonging to the appropriate domain. $S_C^A = \{\xi \in Y : \xi_1 = \tilde{F}^A(\hat{\xi})\}$, $\tilde{F}^A$ is Y_0-periodic. The other notation should be clear from Fig. 1.

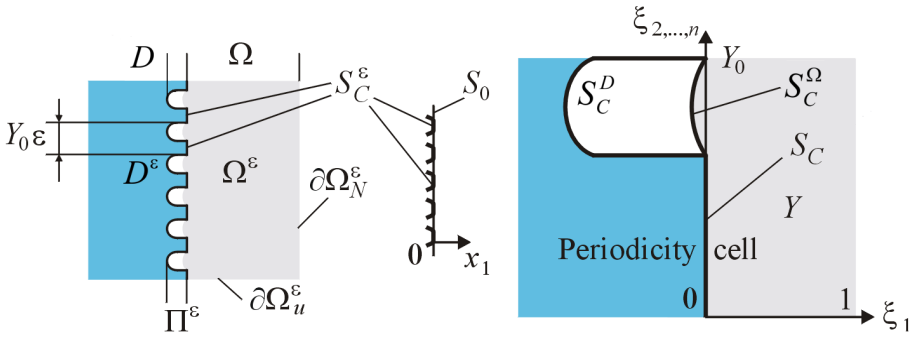

Figure 1: Contact domains and some notation

We consider the case where the domains are bounded and periodic contact conditions are imposed. For the elastic bodies occupying the domains Ω^ε, D^ε, denote by $(\sigma_{ij}^\varepsilon(x))_{n\times n}$ the stress tensor, $(u_i^\varepsilon(x))_n$ the displacement vector, and $(a_{ijkl}(x))$ the n-dimensional symmetric 4-order tensor of elastic constants at a point $x \in \Omega^\varepsilon \cup D^\varepsilon$ and $a_{ijkl}(x) := \chi_{\Omega^\varepsilon} a_{ijkl}^\Omega + \chi_{D^\varepsilon} a_{ijkl}^D$, where χ_Ω is the characteristic function of Ω.

As usual in contact problems (see Chap.6 [12]), later on, we will identify the two surfaces $S_C^{\Omega\varepsilon}$ and $S_C^{D\varepsilon}$ with their projection S_C^ε on the surface $x_1 = 0$; S_0^Ω and S_0^D with their projection S_0; S_C^Ω and S_C^D with their projection S_C on $\xi_1 = 0$.

We write out the equilibrium equations and constitutive elastic relations with contact and boundary conditions:

$$\frac{\partial \sigma_{ij}^\varepsilon(x)}{\partial x_j} = f_i(x), \quad \sigma_{ij}^\varepsilon(x) = a_{ijkl}\frac{\partial u_k^\varepsilon(x)}{\partial x_l}, \qquad x \in \Omega^\varepsilon \cup D^\varepsilon, \tag{1}$$

$$u_{\rm n}^{R\varepsilon}(x) \le g^\varepsilon(x), \qquad \sigma_{\rm n}^\varepsilon(x) \le 0, \qquad \sigma_{\rm n}^\varepsilon(x)\left(u_{\rm n}^{R\varepsilon}(x) - g^\varepsilon(x)\right) = 0 \qquad x \in S_{\rm C}^\varepsilon,$$

$$|\sigma_{\rm it}^\varepsilon(x)| < \mu_i(u_t^\varepsilon)|\sigma_{\rm n}^\varepsilon(x)|, \qquad \Rightarrow \qquad u_{\rm it}^{R\varepsilon} = 0, \qquad x \in S_{\rm C}^\varepsilon, \tag{2}$$

$$\sigma_{\rm it}^\varepsilon = -\mu_i(u_t^\varepsilon)|\sigma_{\rm n}(u^\varepsilon)|\frac{u_{\rm it}^\varepsilon}{|u^\varepsilon|}, \ \Rightarrow \ \text{there } \exists\ \lambda \ge 0 \text{ such that } u_{\rm it}^{R\varepsilon} = -\lambda\sigma_{\rm it}^\varepsilon, \ x \in S_{\rm C}^\varepsilon,$$

$$\sigma_{ij}^\varepsilon n_j(x) = t_i(x) \quad x \in \partial\Omega_{\rm N}^\varepsilon \cup \partial D_{\rm N}^\varepsilon; \ \ u_i^\varepsilon(x) = g_{i0}(x), \quad x \in \partial\Omega_u^\varepsilon \cup \partial D_{\rm u}^\varepsilon. \tag{3}$$

Here, $\sigma_{\rm n}^\varepsilon(x) = \sigma_{ij}^\varepsilon(x)n_j^\varepsilon(x)n_i^\varepsilon(x)$ is the normal stress, $\sigma_{\rm it}^\varepsilon(x) = \sigma_{ij}^\varepsilon(x)n_j^\varepsilon(x) - \sigma_{\rm n}^\varepsilon n_i^\varepsilon(x)$ are the components of the tangential stress vector, $u^{R\varepsilon}(x) := u^\varepsilon(x)|_{S_C^{D\varepsilon}} - u^\varepsilon(x)|_{S_C^{\Omega\varepsilon}}$, $u_{\rm n}^{R\varepsilon}(x) = u_i^{R\varepsilon}(x)n_i(\frac{x}{\varepsilon})$ is the jump in the normal displacement, $u_{\rm it}^{R\varepsilon}(x) = u_i^{R\varepsilon}(x) - u_{\rm n}^{R\varepsilon}n_i^\varepsilon(x)$ are the jumps in the tangential displacements, μ is the friction coefficient ($\mu = 0$ in the case of pure sliding), $n_i^\varepsilon(x) = n_i(x, \frac{x}{\varepsilon})$ are the components of the unit outward normal to the contact interface (more presizely to the boundary $S_C^{D\varepsilon}$), $g^\varepsilon(x) = g\Big(x, \frac{x}{\varepsilon}\Big)$ is the initial gap between contacting surfaces, g_{i0} and t_i are components of prescribed vectors of the boundary displacements and tractions, the latin subscripts assume the values from 1 to n. It is easy to verify (and is derived in [12]) that the normal vector components $(n_1^\varepsilon, n_2^\varepsilon, ..., n_n^\varepsilon)$ as well as the initial gap g^ε can be expressed in terms of the parametrically prescribed contacting surfaces $x_1 - \Phi^A(x_2, ..., x_n) - \varepsilon F^A(x_2, ..., x_n, \frac{x_2}{\varepsilon}, ..., \frac{x_n}{\varepsilon}) = 0$, $A := \{\Omega, D\}$ as the following:

$$\mathbf{n}^\varepsilon = (n_1^\varepsilon, n_2^\varepsilon, ..., n_n^\varepsilon) \equiv \left(1, -\nabla_{\hat x}\Phi^D - \nabla_{\hat\xi}F^D\right)\Big/\sqrt{1 + \left(\nabla_{\hat x}\Phi^D + \nabla_{\hat\xi}F^D\right)^2} \text{ on } S_C^{D\varepsilon}; \tag{4}$$

$$g^\varepsilon = \left(\Phi^\Omega - \Phi^D + \varepsilon(F^\Omega - F^D)\right)\Big/\sqrt{1 + \left(\nabla_{\hat x}\Phi^D + \nabla_{\hat\xi}F^D\right)^2} \tag{5}$$

Furthermore, in the case prescribed on the figure above g^ε depend only on the microstructure and is independent of the macrovariable $\hat x$. In this case, $g^\varepsilon \sim O(\varepsilon)$ and can be modeled as $g^\varepsilon(\hat x) := \varepsilon\bar g\Big(\frac{\hat x}{\varepsilon}\Big)$ with $\bar g \sim O(1)$. In the case, when the surfaces do not coincide on the macro-level along the complete contact zone and S_0 does not coincide with $\{x \in \mathbb{R}^n : \ x_1 = 0\}$, i.e., in the general case, the function g depends on both micro and macro variables and can be represented as a sum $g^\varepsilon(\hat x) = g_0(\hat x) + \varepsilon\bar g\Big(\hat x, \frac{\hat x}{\varepsilon}\Big)$.

Relations (1)–(3) represent the strong formulation of the problem, which applies to smooth domains as well as smooth elastic coefficients and right-hand side functions (prescribed volume forces, boundary displacements, and tractions). Since we deal with nonsmooth domains and allow nonsmooth functions and intend to adopt the finite element method for numerical solution, we rewrite the problem in a weak (variational) formulation.

For any test function from the cone $\mathcal{K}^\varepsilon := \{v = (v_i)_n, v_i \in H^1(\Omega^\varepsilon \cup D^\varepsilon)|\ v_i(x) = g_{0i}(x)$ for $x \in \partial\Omega_u^\varepsilon \cup \partial D_u^\varepsilon$ and $v_n^R \le g^\varepsilon$ on $S_C^\varepsilon\}$, the solution $(u_i^\varepsilon)_n$ of problem (1)–(3) must satisfy the following variational inequality:

$$\int_{\Omega^\varepsilon \cup D^\varepsilon} a_{ijkl}\frac{\partial u_k^\varepsilon(x)}{\partial x_l}\frac{\partial(v_i(x) - u_i^\varepsilon(x))}{\partial x_j}\,dx + \int_{S_{\rm C}^\varepsilon}\mu_i(u_t^\varepsilon)|\sigma_{\rm n}(u^\varepsilon, x)|(|v_{\rm it}^R(x)| - |u_{\rm it}^{R\varepsilon}(x)|)\,ds$$

$$\geq \int_{\Omega^\varepsilon \cup D^\varepsilon} f_i(x)(v_i(x) - u_i^\varepsilon(x))dx + \int_{\partial\Omega_N^\varepsilon \cup \partial D_N^\varepsilon} t_i(x)(v_i(x) - u_i^\varepsilon(x))ds. \tag{6}$$

2.2 A Reduced Variational Inequality

Like in [7] and [12], we assume the following simplification: in the non-convex surface integral

$$\int_{S_C^\varepsilon} \mu_i(u_t^\varepsilon)|\sigma_{\rm n}(u^\varepsilon, x)|(|v_{\rm it}^R| - |u_{\rm it}^{R\varepsilon}|)\, ds.$$

We replace in (6) the friction force, $\mu_i(u_t^\varepsilon)|\sigma_{\rm n}(u^\varepsilon)|$, by some given force $G_i^\varepsilon(x) := G_i(x, \frac{x}{\varepsilon})$. Physically, this corresponds to a situation in which sliding of the frictional surface occurs when components of the frictional stress vector σ_{it}^ε exceed a given function independent of the deformation normal to the contact surface, or the normal stress $\sigma_n(\mathbf{u})$ is prescribed on the real contact area $S_C^{\varepsilon\, real} \subset S_C^\varepsilon$ (see Sec.10.3 [12]). This can be considered as a "first approximation" of the interface shear behavior. Nevertheless, we will keep notation S_C^ε on the place of $S_C^{\varepsilon\, real}$ in the frictional functional of the variational formulation for a moment.

2.3 Auxiliary Results for Descriptions of Boundary Conditions in Terms of Cones in Sobolev Spaces

All the following results are formulated and proved in [16].

Lemma 1 *A set $\mathcal{K} \subset \mathbb{R}^{\mathbf{n}}$ is a closed convex cone in $\mathbb{R}^n$ if and only if it can be represented in the form $\mathcal{K} = \{\eta :\ \mathbf{g}(\eta) = 0\}$, where $\mathbf{g} :\ \mathbb{R}^n \to \mathbb{R}^n$ is the mapping with the following properties:*
(i) $|\mathbf{g}(\eta^1) - \mathbf{g}(\eta^2)| \leq c_0|\eta^1 - \eta^2|,\ \ \forall \eta^1, \eta^2 \in \mathbb{R}^n$;
(ii) $(\mathbf{g}(\eta^1) - \mathbf{g}(\eta^2))(\eta^1 - \eta^2) \geq 0,\ \ \forall \eta^1, \eta^2 \in \mathbb{R}^n$;
(iii) $\eta^0\mathbf{g}(\eta^0) = 0 \Rightarrow \mathbf{g}(\eta^0) = 0,\ \eta^0\mathbf{g}(\eta) \leq 0,\ \ \forall \eta \in \mathbb{R}^n$.

Lemma 2 *Let Ω be a bounded Lipschitz domain and let $\mathbf{g}(\eta, x)$ be a vector field on $\mathbb{R}^n \times \partial\Omega$, measurable in x for each η and satisfying the conditions (i)-(iii) of the previous Lemma in η for almost all x, with the constant c_0 independent of $x \in \partial\Omega$. Then*

$$\mathcal{K} = \{\mathbf{v} \in (H^1(\Omega))^n :\ \mathbf{g}(\mathbf{v}(x), x) = 0 \text{ a.e. on } \partial\Omega\}$$

is a closed convex cone in $(H^1(\Omega))^n$, which coincides with each set

$$\mathcal{K}^1 = \{\mathbf{v} \in (H^1(\Omega))^n :\ \int_{\partial\Omega} \mathbf{g}(\mathbf{v}(x), x) \cdot \mathbf{v}(x)ds = 0\},$$

$$\mathcal{K}^2 = \{\mathbf{v} \in (H^1(\Omega))^n :\ \mathbf{g}(\mathbf{v}(x), x) \cdot \mathbf{v}(x) = 0 \text{ a.e. on } \partial\Omega\}.$$

2.4 Approximation of the Variational Inequality to the Contact Problem by Penalization

As in Sec.3.5, 6 [12] and [6], we replace the constrain inequality $v_n^R \leq g$ in the set of admissible functions by adding the penalty functional

$$\int_{S_C^\varepsilon} b^{\varepsilon,\delta}(x)[u_{\rm n}^{R\varepsilon,\delta}(x) - g^\varepsilon(x)]_+(v_{\rm n}^R - u_{\rm n}^{R\varepsilon,\delta})\, ds, \tag{7}$$

with $b^{\varepsilon,\delta}(x) := \frac{1}{\delta} b\Big(\hat{x}, \frac{x}{\varepsilon}\Big)$ with a real small parameter $\delta > 0$ and $[\cdot]_+ := \max\{0, \cdot\}$ to the left-hand side of (6). In the mechanical sense, it is equivalent to the Winkler-type contact condition, where the surface pressure is proportional to the jump in the normal displacement with some constant coefficient, which is called contact stiffness, i.e., $\sigma_n(u^{\varepsilon,\delta}) = -\frac{1}{\delta} b(\hat{x}, \frac{x}{\varepsilon})[u_i^{R\varepsilon,\delta}(x) n_i^\varepsilon(x) - g^\varepsilon(x)]_+$.
It is easy to verify (see also Ex.2.3 [16]) that the assumptions of Lemma 2 hold for

$$\mathbf{g}(u^{\varepsilon,\delta}(x), x) := \sigma_n(u^{\varepsilon,\delta}) n^\varepsilon(x).$$

Denote $\mathcal{V} = \{v_i \in H^1(\Omega^\varepsilon \cup D^\varepsilon),\ i = 1, ..., n \mid v_i(x) = g_{0i}(x),\ x \in \partial\Omega_u^\varepsilon \cup \partial D_u^\varepsilon\}$. Then, the variational inequality (6) can be rewritten in the form
Find $u_i^{\varepsilon,\delta} \in \mathcal{V}$ such that for all $v_i \in \mathcal{V}$

$$\begin{aligned} &\int_{\Omega^\varepsilon \cup D^\varepsilon} a_{ijkl} \frac{\partial u_k^{\varepsilon,\delta}(x)}{\partial x_l} \frac{\partial (v_i(x) - u_i^{\varepsilon,\delta}(x))}{\partial x_j}\, dx \qquad (8)\\ &+ \int_{S_{\mathrm{C}}^\varepsilon} b^{\varepsilon,\delta}(x)[u_{\mathrm{n}}^{R\varepsilon,\delta}(x) - g^\varepsilon(x)]_+ (v_{\mathrm{n}}^R - u_{\mathrm{n}}^{R\varepsilon,\delta})\, ds + \int_{S_{\mathrm{C}}^\varepsilon} G_i^\varepsilon(x)(|v_{i\mathrm{t}}^R(x)| - |u_{i\mathrm{t}}^{R\varepsilon,\delta}(x)|)\, ds\\ &\geq \int_{\Omega^\varepsilon \cup D^\varepsilon} f_i(x)(v_i(x) - u_i^{\varepsilon,\delta}(x))dx + \int_{\partial\Omega_N^\varepsilon \cup \partial D_N^\varepsilon} t_i(x)(v_i(x) - u_i^{\varepsilon,\delta}(x))ds. \end{aligned}$$

Since the tensor of elastic coefficients is symmetric and the functions under the interface integrals ($[\cdot]_+$ and $|\cdot|$) are convex, problem (8) is equivalent to the minimization of the functional

$$\begin{aligned} I^{\varepsilon,\delta}(v) = &\frac{1}{2}\int_{\Omega^\varepsilon \cup D^\varepsilon} a_{ijkl} \frac{\partial v_k(x)}{\partial x_l} \frac{\partial v_i(x)}{\partial x_j}\, dx + \frac{1}{2\delta}\int_{S_{\mathrm{C}}^\varepsilon} b(\hat{x}, \frac{x}{\varepsilon})[v_{\mathrm{n}}^R(x) - g^\varepsilon(x)]_+^2\, ds\\ &+ \int_{S_{\mathrm{C}}^\varepsilon} G_i^\varepsilon(x)|v_{i\mathrm{t}}^R(x)|\, ds - \int_{\Omega^\varepsilon \cup D^\varepsilon} f_i(x) v_i(x) dx - \int_{\partial\Omega_N^\varepsilon \cup \partial D_N^\varepsilon} t_i(x) v_i(x) ds \qquad (9) \end{aligned}$$

on the set of $v_i \in \mathcal{V}$.

2.5 Incorporation of Dirichlet Boundary Conditions and Jumps in Displacement on the Contact Interface

As in [14], the non-linear Dirichlet conditions and interface jumps g^ε can be incorporated by introduction of a vector-function $\tilde{\mathbf{g}}^\varepsilon = \{\tilde{g}_j^\varepsilon\}_{j=1}^n$, $\tilde{g}_j^\varepsilon \in H^1(\Omega^\varepsilon \cup D^\varepsilon)$, such that $\{\tilde{g}_i^\varepsilon|_{\partial\Omega_u^\varepsilon \cup \partial D_u^\varepsilon} = g_{i0},\ \tilde{\mathbf{g}}^\varepsilon \cdot \mathbf{n}|_{S_C^{\varepsilon+}} - \tilde{\mathbf{g}}^\varepsilon \cdot \mathbf{n}|_{S_C^{\varepsilon-}} = g^\varepsilon;\ \tilde{\mathbf{g}}^\varepsilon \cdot \tau|_{S_C^{\varepsilon+}} - \tilde{\mathbf{g}}^\varepsilon \cdot \tau|_{S_C^{\varepsilon-}} = 0\}$. According to Theorem 22 from [14] such a function can be found satisfying estimate

$$||\tilde{g}_i^\varepsilon||_{H^1(\Omega^\varepsilon \cup D^\varepsilon)} \leq K(||g_{i0}||_{H^{1/2}(\partial\Omega_u^\varepsilon \cup \partial D_u^\varepsilon)} + ||g^\varepsilon||_{H^{1/2}(S_C^\varepsilon)}). \qquad (10)$$

Then, the components of vector-function $\hat{\mathbf{u}}^\varepsilon := \{u_i^\varepsilon - \tilde{g}_i^\varepsilon\}_{i=1}^n$ will belong to $H_0^1(\Omega^\varepsilon \cup D^\varepsilon, \partial\Omega_u^\varepsilon \cup \partial D_u^\varepsilon)$, where $H_0^1(\Omega, \partial\Omega_u) := \{v \in H^1(\Omega) |\ v = 0 \text{ on } \partial\Omega_u\}$.
Now, the weak formulation of the contact problem (8) can be rewritten as the following:

$$\begin{aligned} &\int_{\Omega^\varepsilon \cup D^\varepsilon} a_{ijkl}(x) \frac{\partial \hat{u}_k^{\varepsilon,\delta}(x)}{\partial x_l} \frac{\partial (v_i(x) - \hat{u}_i^{\varepsilon,\delta}(x))}{\partial x_j}\, dx + \int_{S_{\mathrm{C}}^\varepsilon} b^{\varepsilon,\delta}(x)[\hat{u}_{\mathrm{n}}^{R\varepsilon,\delta}(x)]_+ (v_{\mathrm{n}}^R - \hat{u}_{\mathrm{n}}^{R\varepsilon,\delta})\, ds\\ &+ \int_{S_{\mathrm{C}}^\varepsilon} G_i^\varepsilon(x)(|v_{i\mathrm{t}}^R(x)| - |\hat{u}_{i\mathrm{t}}^{R\varepsilon,\delta}(x)|)\, ds \geq \int_{\Omega^\varepsilon \cup D^\varepsilon} \Big(f_i(x)(v_i(x) - \hat{u}_i^{\varepsilon,\delta}(x)) \qquad (11)\\ &- a_{ijkl}(x) \frac{\partial \tilde{g}_k^\varepsilon(x)}{\partial x_l} \frac{\partial (v_i(x) - \hat{u}_i^{\varepsilon,\delta}(x))}{\partial x_j}\Big) dx + \int_{\partial\Omega_N^\varepsilon \cup \partial D_N^\varepsilon} t_i(x)(v_i(x) - \hat{u}_i^{\varepsilon,\delta}(x))ds, \end{aligned}$$

for all $v_i \in H_0^1(\Omega^\varepsilon \cup D^\varepsilon, \partial\Omega_u^\varepsilon \cup \partial D_u^\varepsilon)$.
This is equivalent to the minimization of the functional

$$I^{\varepsilon,\delta}(v) = \frac{1}{2}\int_{\Omega^\varepsilon \cup D^\varepsilon} a_{ijkl}(x)\frac{\partial v_k(x)}{\partial x_l}\frac{\partial v_i(x)}{\partial x_j}\,dx + \frac{1}{2\delta}\int_{S_{\rm C}^\varepsilon} b(\hat{x},\frac{x}{\varepsilon})[v_{\rm n}^R(x)]_+^2\,ds$$
$$+ \int_{S_{\rm C}^\varepsilon} G_i^\varepsilon(x)|v_{it}^R(x)|\,ds - \int_{\Omega^\varepsilon \cup D^\varepsilon}\left(f_i(x)v_i(x) - a_{ijkl}(x)\frac{\partial \tilde{g}_k^\varepsilon(x)}{\partial x_l}\frac{\partial v_i(x)}{\partial x_j}\right)dx$$
$$- \int_{\partial\Omega_N^\varepsilon \cup \partial D_N^\varepsilon} t_i(x)v_i(x)ds \qquad (12)$$

on the set of $v_i \in H_0^1(\Omega^\varepsilon \cup D^\varepsilon, \partial\Omega_u^\varepsilon \cup \partial\Omega_u^\varepsilon)$.

We can choose $\tilde{\mathbf{g}}^\varepsilon$ as shown in the following example.

Example 3 *Let* $g_{0i}(x)|_{\partial\Omega_u^\varepsilon \cup \partial D_u^\varepsilon} = 0$.
$\tilde{\mathbf{g}}^\varepsilon :=^t (\tilde{g}(\frac{x}{\varepsilon}), \underbrace{0,...,0}_{n-1})$, *where* $\tilde{g}(x) = -(\psi(x_1)g_0(x) + \varepsilon\phi(x_1)\bar{g}(\frac{\hat{x}}{\varepsilon}))\sqrt{1+|\nabla_{\hat{x}}\Phi^D + \nabla_{\hat{\xi}}F^D|^2}$
with

$$g_0(\hat{x})|_{x\in\Omega^\varepsilon\cup D^\varepsilon} = \begin{cases} g_0(x) & \text{for } x_1 = \Phi^D(\hat{x}) \cap \{\hat{x}\in\Omega\cup D\};\\ 0 & \text{for } \{x_1 < \Phi^D(\hat{x})\}\cup\{\Phi^D(\hat{x}) < x_1\}\cap\{\hat{x}\in\Omega\cup D\},\end{cases}$$

$$\bar{g}(\frac{\hat{x}}{\varepsilon})|_{x\in\Omega^\varepsilon\cup D^\varepsilon} = \begin{cases} \bar{g}(\frac{\hat{x}}{\varepsilon}) & \text{for } x_1 = \Phi^D(\hat{x}) + \varepsilon F^D(\frac{\hat{x}}{\varepsilon})\cap\{\hat{x}\in\Omega\cup D\};\\ 0 & \text{for } \{x_1 < \Phi^D(\hat{x}) + \varepsilon F^D(\frac{\hat{x}}{\varepsilon})\}\cup\{\Phi^D(\hat{x}) + \varepsilon F^D(\frac{\hat{x}}{\varepsilon}) < x_1\}\\ & \quad\cap\{\hat{x}\in\Omega\cup D\},\end{cases}$$

and $\psi,\ \phi \in C_0^\infty(\mathbb{R}^1)$,

$$\psi(x_1) = \begin{cases} 1 & \text{for } \Phi^D(\hat{x}) - Y_0/3 \le x_1 \le \Phi^D(\hat{x}) + Y_0/3;\\ 0 & \text{for } \{x_1 < \Phi^D(\hat{x}) - 2Y_0/3\}\cup\{\Phi^D(\hat{x}) + 2Y_0/3 < x_1\},\end{cases}$$

$$\phi(x_1) = \begin{cases} 1 & \text{for } \Phi^D(\hat{x}) - \varepsilon Y_0/2 \le x_1 \le \Phi^D(\hat{x}) + \varepsilon Y_0/2;\\ 0 & \text{for } \{x_1 < \Phi^D(\hat{x}) - \varepsilon Y_0\}\cup\{\Phi^D(\hat{x}) + \varepsilon Y_0 < x_1\}.\end{cases}$$

2.6 Existence and Preliminary Estimate for the Solution of the Microcontact Problem

The following theorem yields the existence and preliminary estimates to the solution of the contact problem (6) and is presented by Theorems 2.2 and 2.3 in [7] or by Th. 5.1 in [5]:

Theorem 4 *If measures of* $\partial\Omega_u^\varepsilon, \partial D_u^\varepsilon$ *are positive,* $f \in (L^2(\Omega^\varepsilon\cup D^\varepsilon))^n$, $t \in (L^2(\partial\Omega_N^\varepsilon \cup \partial D_N^\varepsilon))^n$, $g^\varepsilon \in H^{1/2}(S_C^\varepsilon)$ *(*$g_0 \in H^{1/2}(S_C^0)$, $\bar{g} \in H_{per}^{1/2}(S_C, C(\bar{\Omega}\cup\bar{D}))$*),* b^ε, $G_i^\varepsilon \in L^\infty(S_C^\varepsilon)$, $b \ge \alpha > 0$, $G_i^\varepsilon \ge 0$ *and* $a_{ijkl} \in L^\infty(\Omega^\varepsilon\cup D^\varepsilon)(i,j,k,l = 1,...,n)$*, the tensor of elastic constants* $(a_{ij}^{hk}(x))$ *is symmetric at each point* $x \in \Omega^\varepsilon$*:*

$$a_{ijkl}(x) = a_{jilk}(x) = a_{ljil}(x) = a_{ilkj}(x) \qquad (13)$$

and positive-definite, with elements bounded at each point $x \in \Omega$*:*

$$c_0\eta_{jk}\eta_{jk} \le a_{hikj}(x)\eta_{ih}\eta_{jk} \le C_0\eta_{jk}\eta_{jk}, \qquad (14)$$

for all $\eta_{jk} = \eta_{kj} \in \mathbb{R}$, where the constants $0 < c_0 \le C_0 < \infty$ are independent of x.
Then, for every $\delta > 0$ and fixed $\varepsilon > 0$, problem (8) has a unique solution in the set of admissible functions $u^{\varepsilon,\delta} \in \mathcal{V}(\Omega^\varepsilon \cup D^\varepsilon))^n$ and this solution satisfies the following estimate

$$||u^{\varepsilon,\delta}||_{H^1(\Omega^\varepsilon \cup D^\varepsilon)} \le c(||f||_{L^2(\Omega^\varepsilon \cup D^\varepsilon)} + ||t||_{L^2(\partial\Omega^\varepsilon_N) \cup \partial D^\varepsilon_N} + ||g_{i0}||_{H^{1/2}(\partial\Omega^\varepsilon_u \cup \partial D^\varepsilon_u)} + ||g^\varepsilon||_{H^{1/2}(S^\varepsilon_C)} + 1), \quad (15)$$

for some constant c depending on measure of domain Ω^ε and constants from the condition of the positive definiteness and boundedness of the tensor of elastic constants $(a_{ijkl})_{n\times n\times n\times n}$, α and G^ε_i $(i = 1, ..., n)$.
Furthermore, there exists a subsequence w.r.t δ of such solutions, that converges weakly in H^1, for every fixed ε, to the unique solution of the constrained problem (6) as $\delta \to 0$.

The proof is based on the convexity and Gateaux-differentiability of the functional $I^{\varepsilon,\delta}(v)$, that imply its weak lower semicontinuity, and the coerciveness of the functional $I^{\varepsilon,\delta}(v)$, which rests on the coerciveness of the bilinear form $a_{\Omega^\varepsilon}(u, v) := \int_{\Omega^\varepsilon} a_{ijkl} \frac{\partial u_k(x)}{\partial x_l} \frac{\partial v_i(x)}{\partial x_j}\, dx$ and Korn's inequality (see Chap. 3 [12] and Th.3.1 [5]).
The following lemma about an extension operator and the boundedness of the right-hand side is proved in [16]:

Lemma 5 *There are linear extension operators $P^\varepsilon : H^1(\Omega^\varepsilon)^n \to H^1(\tilde{\Omega})^n$ from the domain Ω^ε to $\tilde{\Omega} = int(\bar{\Omega} \cup (S^0_C \times [0, 1]))$, such that $\sup_\varepsilon ||P^\varepsilon|| < \infty$.*
Furthermore, the following estimate is valid for the right-hand side: $\sup_\varepsilon ||f^\varepsilon||_{L^2(\Omega^\varepsilon)} < \infty$.

Proposition 6 *The solution to problem (8) is bounded uniformly in ε, i.e. the above estimate in (15) is independent of ε.*

Proof:
Owing to Lemma 5, $\sup_\varepsilon ||f^\varepsilon||_{L^2(\Omega^\varepsilon)} < \infty$.
Consider now function $g^\varepsilon(x)$. Let us refer to Sec.2.5 and consider $g^\varepsilon(x)$ as a trace of a H^1-function $\tilde{g}^\varepsilon$. We want to estimate integral $\int_{\Omega^\varepsilon \cup D^\varepsilon} a_{ij1l} \frac{\partial \tilde{g}^\varepsilon(x)}{\partial x_l} \frac{\partial v_i(x)}{\partial x_j} dx$ from the minimization problem (12).

$$|\int_{\Omega^\varepsilon \cup D^\varepsilon} a_{ij1l} \frac{\partial \tilde{g}^\varepsilon(x)}{\partial x_l} \frac{\partial v_i(x)}{\partial x_j} dx| \le ||a_{ij1l} \nabla_{x_l} \tilde{g}^\varepsilon||_{L^2(\Omega^\varepsilon \cup D^\varepsilon)} ||v||_{H^1(\Omega^\varepsilon \cup D^\varepsilon)}$$

Recall that the sequence $\tilde{g}^\varepsilon(x)(x) = \tilde{g}_0(x) + \varepsilon \tilde{\bar{g}}(x, \frac{x}{\varepsilon})$, where $\tilde{g}_0 \in H^1(\Omega \cup D)$, $\bar{g} \in H^1_{per}(Y, C(\bar{\Pi}^\varepsilon))$, where Π^ε is the layer of the thickness εY_0 around the contact surface S^ε_C. The uniform in ε boundedness of the term $||a_{ij1l} \nabla_{x_l} \tilde{g}_0||_{L^2(\Omega^\varepsilon \cup D^\varepsilon)}$ follows from Lemma 5. Let us denote $Y_m := Y_0 + Y_0 \otimes m$, $m \in \mathbb{Z}^{n-1}$, $\psi(x, \frac{x}{\varepsilon}) := a_{ij1l}(x, \frac{x}{\varepsilon}) \frac{\partial \tilde{\bar{g}}(x, \frac{x}{\varepsilon})}{\partial x_l}$ and show the boundedness for $\varepsilon\psi$ in $L^2(\Omega^\varepsilon \cup D^\varepsilon)$ uniformly in ε:

$$\begin{aligned}
&\sup_\varepsilon \varepsilon \int_{\Omega^\varepsilon \cup D^\varepsilon} |\psi(x, \frac{x}{\varepsilon})|^2 dx \le \\
&\le \sup_\varepsilon \varepsilon \sum_{\varepsilon Y_m \subset \{\Phi^D(\hat{x}) - \varepsilon Y_0/2 \le x_1 \le \Phi^D(\hat{x}) + \varepsilon Y_0/2\}} \int_{\varepsilon Y_m} |\psi(x, \frac{x}{\varepsilon})|^2 dx \\
&= \sup_\varepsilon \sum_{\varepsilon Y_m \subset \{\Phi^D(\hat{x}) - \varepsilon Y_0/2 \le x_1 \le \Phi^D(\hat{x}) + \varepsilon Y_0/2\}} \varepsilon^{n+1} \int_{Y_m} |\psi(x, \xi)|^2 d\xi \\
&\le \sup_\varepsilon \varepsilon^2 \frac{|S^0_C|}{|T|} \int_Y \sup_{x \in S^0_C} |\psi(x, \xi)|^2 d\xi \le \varepsilon^2_{max} \frac{|S^0_C|}{|T|} \int_Y \sup_{x \in S^0_C} |\psi(x, \xi)|^2 d\xi \\
&\le \varepsilon^2_{max} \frac{|S^0_C|}{|T|} \|\psi(x, \xi)\|^2_{L^2(Y, C(\bar{\Pi}^\varepsilon))}.
\end{aligned}$$

Here ε_{max} is the max available value of ε (e.g., we can take $\varepsilon_{max} = 1$). It remains only to recall that $\partial\Omega_N^\varepsilon$, ∂D_N^ε, $\partial\Omega_u^\varepsilon$ and ∂D_u^ε are independent of ε and coinsides with $\partial\Omega_N$, ∂D_N, $\partial\Omega_u$ and ∂D_u.

2.7 Regularization of the friction functional. Approximation of the Variational Inequality by Variational Equation

The major difficulty in numerical solving the problem (8) is caused by the presence of the non-differentiable Euclidean norms $|v_{it}^R|$ and $|u_{it}^{R\varepsilon,\delta}|$. We replace them as in [12], [7] by smooth and convex approximation $\phi^\gamma(v_{it}^R)$

$$\phi^\gamma(v) = \begin{cases} |v| - \frac{1}{2}\gamma & \text{if } |v| \geq \gamma, \\ \frac{1}{2\gamma}|v|^2 & \text{if } |v| < \gamma \end{cases}, \tag{16}$$

$$\sigma_t(\mathbf{u}_t^{R\varepsilon,\delta,\gamma}) = -G_i^\varepsilon \frac{\partial\phi}{\partial \mathbf{u}_t^{R\varepsilon,\delta,\gamma}}(\mathbf{u}_t^{R\varepsilon,\delta,\gamma}) = \begin{cases} -G_i^\varepsilon u_{it}^{R\varepsilon,\delta,\gamma}/|u_t^{R\varepsilon,\delta,\gamma}| & \text{if } |u_{it}^{R\varepsilon,\delta,\gamma}| \geq \gamma, \\ -G_i^\varepsilon u_{it}^{R\varepsilon,\delta,\gamma}/\gamma & \text{if } |u_{it}^{R\varepsilon,\delta,\gamma}| < \gamma. \end{cases} \tag{17}$$

The resulting smooth variational inequality obtained from (6) is equivalent to the following variational equation:
Find $u_i^{\varepsilon,\delta,\gamma} \in \mathcal{V}$ such that for all $v_i \in \mathcal{V}$

$$\begin{aligned} &\int_{\Omega^\varepsilon \cup D^\varepsilon} a_{ijkl} \frac{\partial u_k^{\varepsilon,\delta,\gamma}(x)}{\partial x_l} \frac{\partial v_i(x)}{\partial x_j}\, dx + \int_{S_{\mathrm{C}}^\varepsilon} b^{\varepsilon,\delta}(x)[u_{\mathrm{n}}^{R\varepsilon,\delta,\gamma}(x) - g^\varepsilon(x)]_+ v_{\mathrm{n}}^R\, ds \\ &+ \int_{S_{\mathrm{C}}^\varepsilon} G_i^\varepsilon \frac{\partial\phi}{\partial \mathbf{u}_t^{R\varepsilon,\delta,\gamma}}(\mathbf{u}_t^{R\varepsilon,\delta,\gamma}) v_{it}^R(x)\, ds \\ &= \int_{\Omega^\varepsilon \cup D^\varepsilon} f_i(x) v_i(x) dx + \int_{\partial\Omega_N^\varepsilon \cup \partial D_N^\varepsilon} t_i(x) v_i(x) ds. \end{aligned} \tag{18}$$

Mechanically this approximation means that there is some boundary layer between regions of full stick and slip. that is, for a given small $\gamma > 0$, we set

$$\begin{aligned} |u_{it}^{R\varepsilon,\delta}| < \gamma \qquad &\Rightarrow \text{sticking}, \\ |u_{it}^{R\varepsilon,\delta}| \geq \gamma \qquad &\Rightarrow \text{sliding or slip}. \end{aligned}$$

2.8 Mechanical Interpretation of Approximated Contact Conditions

In this section, we refer to Sec.2.2 and will use the notation $S_C^{\varepsilon\,real}$ for the real contact surface dependent on u_n. It is determined as the following: $S_C^{\varepsilon\,real} := \{x \in S_C^\varepsilon : u_n^{R\varepsilon,\delta,\gamma} \geq g^\varepsilon\}$ and

$$\int_{S_C^{\varepsilon\,real}} \cdot ds = \int_{S_C^\varepsilon} H(u_n^{R\varepsilon,\delta,\gamma}(x) - g^\varepsilon(x)) \cdot ds,$$

where H is the Heaviside function, i.e. $H(v) = 1$ if $v \geq 0$ and $H(v) = 0$ otherwise.
Let us consider three surface integrals appearing in the variational equality (18):

$$\begin{aligned} j_n(v_{\mathrm{n}}^R) + j_t(v_{\mathrm{t}}^R) + j_{fr}(v_{\mathrm{t}}^R) = & \\ = \frac{1}{\delta} \int_{S_{\mathrm{C}}^{\varepsilon\,real}(u_n)} & b(\hat{x}, \frac{x}{\varepsilon}) \left(u_{\mathrm{n}}^{R\varepsilon,\delta,\gamma}(x) - g^\varepsilon(x)\right) v_{\mathrm{n}}^R\, ds \\ + \frac{1}{\gamma} \int_{\{x \in S_{\mathrm{C}}^{\varepsilon\,real}:\, 0 < |u_{it}^{R\varepsilon,\delta}(x)| < \gamma\}} & G_i^\varepsilon u_{it}^{R\varepsilon,\delta,\gamma}(x) v_{it}^R(x)\, ds \\ + \int_{\{x \in S_{\mathrm{C}}^{\varepsilon\,real}:\, |u_{it}^{R\varepsilon,\delta}(x)| \geq \gamma\}} & G_i^\varepsilon \frac{u_{it}^{R\varepsilon,\delta,\gamma}(x)}{|u_t^{R\varepsilon,\delta,\gamma}|} v_{it}^R(x)\, ds. \end{aligned} \tag{19}$$

Functionals $j_n,\ j_t$ describe contact layers of small penetrations δ and γ respectively. This contact layers can be mechanically imaged by springs of stiffnesses $k_n^{\varepsilon,\delta} := b(\hat{x}, \frac{x}{\varepsilon})/\delta$ and $k_\tau^{\varepsilon,\gamma} := G_i^\varepsilon/\gamma$ respectively. $k_n^{\varepsilon,\delta}$ and $k_\tau^{\varepsilon,\gamma}$ are called normal and tangential microcontact stiffnesses. Usually in the mechanical literature, they are taken as the following: $k_n = E/\delta$ and $k_\tau = G/\gamma$, where E is the Young's modulus, G is share modulus of the material, δ and γ are thicknesses of the artificial contact layers. In the part of the real contact with the stick condition, the tangential contact layer with its stiffness is supposed. In the other part of the contact, the frictional traction is supposed, i.e. the tangential tractions are equal to the friction traction G_i^ε. This sliding or slip condition is expressed by functional j_{fr}.

3 Homogenization Procedure and Basic Results

Since problem (1)–(3), as well as its variational formulation (6), has two different size scales on the micro- and macrolevels, it is very difficult to perform its direct numerical solution. So we intend to reduce the problem to a single-scale problem and then numerically solve it. For the scale reduction, asymptotic homogenization was chosen.

3.1 Auxiliary Results

Following definitions and Theorems 7-11 were given by [1].

Definition 7 *A sequence of functions u_ε in $L^2(\Omega)$ is said to two-scale converge to a limit $u_0(x,\xi) \in L^2(\Omega \times Y)$, iff for any function $\psi(x,\xi) \in \mathcal{D}(\Omega, C^\infty_{per}(Y))$, we have*

$$\lim_{\varepsilon\to 0} \int_\Omega u^\varepsilon(x)\psi(x,\frac{x}{\varepsilon})dx = \frac{1}{|Y|}\int_\Omega \int_Y u_0(x,\xi)\psi(x,\xi)dxd\xi. \tag{20}$$

This makes sense because of the next compactness theorem.

Theorem 8 *From each bounded sequence $u_\varepsilon \in L^2(\Omega)$, we can extract a subsequence , which two-scale converges to $u_0(x,\xi) \in L^2(\Omega \times Y)$.*

Theorem 9 *Let u^ε be a sequence that two-scale converges to $u_0(x,\xi)$. Then u^ε weakly converges in $L^2(\Omega)$ to $u_\star(x) = \int_Y u_0(x,\xi)d\xi$, and we have:*

$$\lim_{\varepsilon\to 0} ||u^\varepsilon||_{L^2(\Omega)} \geq \frac{1}{|Y|}||u_0||_{L^2(\Omega\times Y)} \geq ||u_\star||_{L^2(\Omega)}. \tag{21}$$

Furthermore, if equality is achieved in the left part of (21), and $u_0(x,\xi)$ is smooth, then we have

$$\lim_{\varepsilon\to 0} ||u^\varepsilon(x) - u_0(x,\frac{x}{\varepsilon})||_{L^2(\Omega)} = 0. \tag{22}$$

The following lemma is presented in [1], Lemma 1.3. We only replace in its statement $L^2(\Omega, C_{per}(Y))$ by $L^2_{per}(Y, C(\bar{\Omega}))$, owing to remark 1.5 and corollary 5.4 from the same source.

Lemma 10 *Assume that Ω is a bounded open set (its closure $\bar{\Omega}$ is thus compact). Let $\psi(x,\xi)$ be a function in $L^2_{per}(Y, C(\bar{\Omega}))$. Then, $\psi(x,\frac{x}{\varepsilon})$ is a measurable function on Ω for any positive value of ε, and we have*

$$\lim_{\varepsilon\to 0} \int_\Omega \psi(x,\frac{x}{\varepsilon})^2 dx = \frac{1}{|Y|}\int_\Omega \int_Y \psi(x,\xi)^2 dxd\xi. \tag{23}$$

Theorem 11 *Let u_ε be a bounded sequence in $H^1(\Omega)$ that converges weakly to a limit $u \in H^1(\Omega)$. Then, u_ε two-scale converges to $u_0(x,\xi) := u(x)$, and there exists a function $u_1(x,\xi)$ in $L^2(\Omega, H^1_{per}(Y))$ such that, up to a subsequence, ∇u_ε two-scale converges to $\nabla_x u(x) + \nabla_\xi u_1(x,\xi)$.*

Remark 12 *"Converges up to a subsequence" means that the sequence u_ε has a convergent subsequence, $u_{\varepsilon'}$, which we again redenote by u_ε.*

We complete the domain-two-scale convergence with Theorem 2.6 from [1]

Theorem 13 *Assume that $\nabla_\xi u_1(x,\xi)$ is an "admissible" test function in the sense of (23). Then, the sequence $[\nabla u^\varepsilon(x) - \nabla u_0(x) - \nabla_\xi u_1(x, x/\varepsilon)]$ converges strongly to zero in $(L^2(\Omega))^n$.*

The next lemma corresponds to Lemma 2 [17] and yields estimates for oscillating surfaces and boundary layers, which will be used for the proof of the main results of this paper.

Lemma 14 *Any $w \in H^1(\Omega^\varepsilon, \partial\Omega_u)$ satisfies the inequality:*

$$||w||_{L^2(S^\varepsilon_C)} \le c_3(\varepsilon^{-1/2}||w||_{L^2(\Omega)} + \varepsilon^{1/2}||\nabla_x w||_{L^2(\Omega)}). \tag{24}$$

As a next, we introduce the definition of the two-scale convergence on the oscillating surface from [2].

Lemma 15 *The space $B = C(\bar\Omega, C_{per}(Y))$ is a separable Banach space (i.e. it contains a dence countable family), which is dence in $L^2(\Omega, L^2(\mathcal{S}_C))$, and such that any function $\phi(x,\xi) \in B$ satisfies*

$$\varepsilon \int_{S^\varepsilon_C} |\phi(x, \frac{x}{\varepsilon})|^2 ds \le C||\phi||^2_B,$$

and

$$\lim_{\varepsilon\to 0} \varepsilon \int_{S^\varepsilon_C} |\phi(x, \frac{x}{\varepsilon})|^2 ds = \int_\Omega \int_{S_C} |\phi(x,\xi)|^2 ds_\xi ds.$$

Proposition 16 *Let u^ε be a sequence of functions in $H^1(\Omega)$ such that*

$$||u^\varepsilon||_{L^2(\Omega)} + \varepsilon||\nabla u^\varepsilon||_{L^2(\Omega)} \le C,$$

where C is a posotiv constant independent of ε and u^ε two-scale converges to $u^0(x,\xi) \in L^2(\Omega, H^1_{per}(Y))$. Then, the trace of u^ε on S^ε_C satisfies the estimate

$$\varepsilon \int_{S^\varepsilon_C} |u^\varepsilon(x)|^2 ds \le C,$$

and

$$\lim_{\varepsilon\to 0} \varepsilon \int_{S^\varepsilon_C} u^\varepsilon(x)\phi(x, \frac{x}{\varepsilon}) ds = \int_\Omega \int_{S_C} u^0(x,\xi)\phi(x,\xi) ds_\xi ds,$$

$$\lim_{\varepsilon\to 0} \varepsilon \int_\Omega \nabla u^\varepsilon(x)\phi(x, \frac{x}{\varepsilon}) ds = \int_\Omega \int_Y \nabla_\xi u^0(x,\xi)\phi(x,\xi) ds_\xi ds.$$

for any continuous function $\phi(x,\xi) \in C(\bar\Omega, C_{per}(Y))$.

The following proposition is based on the lower semicontinuity of the form $a_{\Omega_0}(v,v)$ with respect to the weak convergence in $(H^1(\Omega))^n$ (see A1.1 [9], [16]):

Proposition 17 *For any sequence $v^\varepsilon \rightharpoonup v$ in $(H^1(\Omega))^n$, we have*

$$\liminf_{\varepsilon\to 0} a_{\Omega_\varepsilon}(v^\varepsilon, v^\varepsilon) \geq \liminf_{\varepsilon\to 0} a_{\Omega_0}(v^\varepsilon, v^\varepsilon) \geq a_{\Omega_0}(v, v),$$

since the form $a_{\Omega_0}(v, v)$ is lower semicontinuous with respect to weak convergence in $(H^1(\Omega))^n$.

The following Lemma yields convergence for the surface integrals and can be found as Lemma 5.4 in [16]:

Lemma 18 *Let $\mathbf{g}^\varepsilon(\eta, y)$ defined on $\mathbb{R}^n \times S_C^\varepsilon$ satisfies the inequalities:*

$$|\mathbf{g}^\varepsilon(\eta, y_1) - \mathbf{g}^\varepsilon(\eta, y_2)| \leq \mu(1 + |\eta|)|y^1 - y^2|, \qquad \forall y^1, y^2 \in S_C^\varepsilon, \eta \in \mathbb{R}^n,$$
$$\sup_{y\in\Omega} |\mathbf{g}^\varepsilon(\eta^1, y) - \mathbf{g}^\varepsilon(\eta^2, y)| \leq \mu|\eta^1 - \eta^2|, \qquad \forall \eta^1, \eta^2 \in \mathbb{R}^n,$$

where μ is a positive constant, and has almost everywhere on S_C^ε the representation: $\mathbf{g}^\varepsilon(\eta, x) = \mathbf{g}(\eta, \hat{x}, \varepsilon^{-1}x)$. Then for any sequences $u^\varepsilon \in (H^1(\Omega))^n$, $v^\varepsilon \in H^1(\Omega)$ such that $u^\varepsilon \rightharpoonup u^0$, $v^\varepsilon \rightharpoonup v^0$ as $\varepsilon \to 0$, we have the convergence:

$$\int_{S_C^\varepsilon} \mathbf{g}^\varepsilon(u^\varepsilon(x), x)v^\varepsilon(x)ds \to \int_{S_0} \left(\frac{1}{|T|}\int_{S_C} \mathbf{g}(u^0(0, \hat{x}), \hat{x}, \xi)ds_\xi\right) v^0(0, \hat{x})d\hat{x}, \qquad (25)$$

where $|T|$ stands for the measure of the domain T.

The following Lemma claims that the limiting function defines a closed convex cone and can be found as Lemma 5.5 in [16].

Lemma 19 *Let $\mathbf{g}^\varepsilon(\eta, y)$ be a given sequence from the previous Lemma, satisfying all requirements of Lemma 1 and w.r.t. Lemma 2*

$$\mathcal{K}^\varepsilon = \{\mathbf{v} \in (H^1(\Omega^\varepsilon \cup D^\varepsilon))^n : \ \mathbf{g}^\varepsilon(\mathbf{v}(x), x) = 0 \text{ a.e. on } S_C^\varepsilon\}$$

be a closed convex cone in $(H^1(\Omega^\varepsilon \cup D^\varepsilon))^n$. And let $\mathbf{g}^0(\eta, y) := \frac{1}{|T|}\int_{S_C} \mathbf{g}(\eta, \hat{x}, \xi)ds_\xi$ be its waited mean value in the fast variable. Then $\mathbf{g}^0(\eta, y)$ defines a closed convex cone in $(H^1(\Omega \cup D))^n$, namely,

$$\mathcal{K}^0 = \{\mathbf{v} \in (H^1(\Omega \cup D))^n : \ \mathbf{g}^0(\mathbf{v}(\hat{x}, 0), \hat{x}) = 0 \text{ a.e. on } S_0\}.$$

Moreover, if $\mathbf{v}^\varepsilon \in \mathcal{K}^\varepsilon$ converges weakly to some $\mathbf{v^0} \in (H^1(\Omega \cup D))^n$, then $\mathbf{v^0}|_{\Omega\cup D} \in \mathcal{K}^0$.

Lemma 20 *Let $\bar{\Omega}'$ be a fixed subdomain of Ω with Lipschitz continuous boundary, and $\mathbf{g}(\eta, x, \xi)$ be a sequence defined on $\mathbb{R}^n \times \bar{\Omega}' \times S_C$ satisfying the required in Lemma 18 inequalities by taking of $\sup_{\xi\in S_C}$ from their left-hand sides. Then for any sequences $u^\varepsilon \in (H^1(\Omega))^n$, $v^\varepsilon \in H^1(\Omega)$ such that $u^\varepsilon \rightharpoonup u^0$, $v^\varepsilon \rightharpoonup v^0$ as $\varepsilon \to 0$, we have the convergence:*

$$\varepsilon\int_{S_C^\varepsilon\cap\Omega'} \mathbf{g}^\varepsilon(u^\varepsilon(x), x)v^\varepsilon(x)ds \to \frac{1}{|Y|}\int_{\Omega'}\int_{S_C} \mathbf{g}(u^0(x), x, \xi)ds_\xi v^0(x)dx. \qquad (26)$$

3.2 Homogenization of Contact Conditions

This section is generally based on the application of Lemma 18.

Remark 21 *Note that the assumption $u^\varepsilon \in (H^1(\Omega))^n$, $v^\varepsilon \in H^1(\Omega)$ from Lemma 18 are in general not satisfied for a solution of a contact problem, since the solution is from $(H^1(\Omega \cup D))^n$ with possible jumps $g^\varepsilon \in H^{1/2}(S_C^\varepsilon)$ on the contact interface. Nevertheless, Lemma 18 can be applied, since the Trace theorem as well as the Gauss theorem in the counterparts of its proof can be replaced by analogous theorems for jumps (see The. 22, 19 [14]).*

3.2.1 Homogenization of the Non-penetration Condition

We suppose in this subsection that there is no micro-friction, i.e., $G_i^\varepsilon = 0$, $i = 1, ..., n$. We consider the contact integral

$$\int_{S_C^\varepsilon} b^{\varepsilon,\delta}(x)[u_i^{R\varepsilon,\delta}(x) \cdot n_i^\varepsilon(x) - g^\varepsilon(x)]_+ n_i^\varepsilon(x) \cdot v_i(x)\, ds. \tag{27}$$

As we already mentioned in the previous section, in our problem, $\mathbf{g}^{\varepsilon,\delta}(u^\varepsilon(x), x) := b^{\varepsilon,\delta}(x)[u^{R\varepsilon,\delta}(x) \cdot n^\varepsilon(x) - g^\varepsilon(x)]_+ n^\varepsilon(x)$. Owing to estimate (15) and Proposition 6, the assumptions of Theorems 8 and 9 are satisfied for $u_{\mathrm{n}}^{\varepsilon,\delta}(x)$ for each fixed δ.
Consider now function $g^\varepsilon(x)$. Let us refer to Sec.2.5 and consider $g^\varepsilon(x)$ as a trace of a H^1-function $\tilde{g}^\varepsilon(x)$.
We denote by $H^1_{per}(Y, C(\Pi^\varepsilon)) = \left\{ v \in H^1(Y, C(\bar{\Omega} \cup \bar{D})) :\ v(x,\xi) \text{ is periodic in } \hat{\xi} \text{ and compactly supported in } x \in \Pi^\varepsilon \right\}$.

Lemma 22 *Let $g^\varepsilon \in H^{1/2}(S_C^\varepsilon)$ be a sequence of traces to the sequence $\tilde{g}^\varepsilon(x) = \tilde{g}_0(x) + \varepsilon\tilde{\bar{g}}(x, \frac{x}{\varepsilon})$, where $\tilde{g}_0 \in H^1(\Omega \cup D)$, $\bar{g} \in H^1_{per}(Y, C(\Pi^\varepsilon))$. Then $\tilde{g}^\varepsilon \rightharpoonup \tilde{g}_0$ in H^1.*

Proof:
Consider integral $\int_{\Omega^\varepsilon \cup D^\varepsilon} a_{ij1l} \frac{\partial \tilde{g}^\varepsilon(x)}{\partial x_l} \frac{\partial v_i(x)}{\partial x_j} dx$ from the variational statement (12), where $\tilde{g}^\varepsilon$ is given by Example 3. Since $\tilde{g}_0 \in H^1(\Omega \cup D)$, $\bar{g} \in H^1_{per}(Y, C(\bar{\Pi}^\varepsilon))$, the sequences $a_{ij1l} \frac{\partial \tilde{g}_0(x)}{\partial x_l}$ and $\varepsilon a_{ij1l} \frac{\partial \tilde{\bar{g}}(x, \frac{x}{\varepsilon})}{\partial x_l}$ belong to $L^2(\Omega \cup D)$ and $L^2_{per}(Y, C(\bar{\Pi}^\varepsilon))$ respectively. Hence, owing to Lemma 10, they satisfy the following

$$\lim_{\varepsilon \to 0} \int_{\Omega^\varepsilon \cup D^\varepsilon} (a_{ij1l}(x) \frac{\partial \tilde{g}_0(x)}{\partial x_l})^2 dx = \int_{\Omega \cup D} (a_{ij1l}(x) \frac{\partial \tilde{g}_0(x)}{\partial x_l})^2 dx. \tag{28}$$

$$\lim_{\varepsilon \to 0} \int_{\Omega^\varepsilon \cup D^\varepsilon} (\varepsilon a_{ij1l}(x) \frac{\partial \tilde{\bar{g}}(x, \frac{x}{\varepsilon})}{\partial x_l})^2 dx = \frac{1}{|Y|} \int_{\Omega \cup D} \int_Y (a_{ij1l}(x, \xi) \frac{\partial \tilde{\bar{g}}(x, \xi)}{\partial \xi_l})^2 d\xi dx$$
$$= \frac{1}{|Y|} \int_{\Phi^D(\hat{x}) - \varepsilon Y_0 \le x_1 \le \Phi^D(\hat{x}) + \varepsilon Y_0} \int_Y (a_{ij1l}(x, \xi) \frac{\partial \tilde{\bar{g}}(x, \xi)}{\partial \xi_l})^2 d\xi dx. \tag{29}$$

Owing to Lemma 1 [4], [3] the right-hand side of (29), i.e. the integral over the layer of the thickness $\sim \varepsilon$, tends to $0\ \sim O(\varepsilon)$ as $\varepsilon \to 0$.
According to the uniform in ε estimates obtained for $\int_{\Omega^\varepsilon \cup D^\varepsilon} a_{ij1l} \frac{\partial \tilde{g}^\varepsilon(x)}{\partial x_l} \frac{\partial v_i(x)}{\partial x_j} dx$ in given the proof to Proposition 6, sequence $a_{ij1l} \frac{\partial \tilde{g}^\varepsilon(x)}{\partial x_l}$ is two-scale and weak in L^2 convergent w.r.t. Theorems 8 and 9. Owing to limits in (28) and (29), the two-scale and weak limit of $a_{ij1l} \frac{\partial \tilde{g}^\varepsilon(x)}{\partial x_l}$ is $a_{ij1l} \frac{\partial \tilde{g}_0(x)}{\partial x_l}$. Hence, the statement of the Lemma holds.

Our function $\mathbf{g}^{\varepsilon,\delta}(\eta, x)$ also satisfies assumptions of Lemma 18 (it can be checked or found in Ex.5.6 [16]). Applying Lemma 18 we obtain that

Proposition 23 $\mathbf{g}^{\varepsilon,\delta}(u^\varepsilon(x), x) := b^{\varepsilon,\delta}(x)[u^{R\varepsilon,\delta}(x) \cdot n^\varepsilon(x) - g^\varepsilon(x)]_+ n^\varepsilon(x)$ *converges in the sense of (25) to* $\mathbf{g}^\delta(u^0(0, \hat{x}), \hat{x}, \xi) := \frac{1}{\delta} b(\hat{x}, \frac{\hat{x}}{\varepsilon})[u^{R0,\delta}(x) \cdot n(x, \xi) - g_0(x)]_+ n(x, \xi)$.

Owing to Lemmas 2, 19

Proposition 24 *The homogenized non-penetration constraint condition is the following closed convex cone:*

$$\mathcal{K} := \{\mathbf{v^0} \in (H_0^1(\Omega \cup D, \partial\Omega_u \cup \partial D_u))^n |\ \mathbf{v^{R0}}(x) \cdot n(x, \xi) \le g_0(x), \quad \textit{a.e. in } \xi \in S_C,\ \textit{a.e. on } S_0\} \tag{30}$$

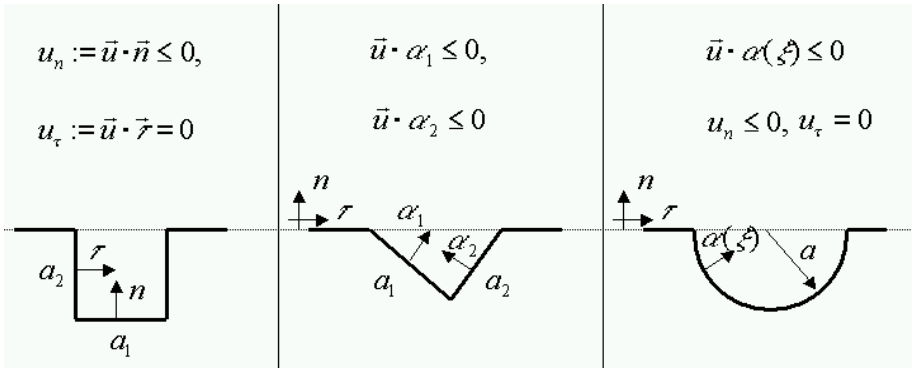

Figure 2: Periodic elements of micro-geometries of stems' surfaces

Recall that this result is contained as an example in the theory of [16] It means that in almost every point of the macrointerface there is a non-penetration condition not only on the normal to the macro-interface direction, but in the fixed cone around the macro-normal. The angle (range) of this cone is relative independent of the hole curvature and length of microvalleys, but is dependent only on the maximal angle between micro- and macro-normal vectors inside the microvalley.

3.2.2 Mechanical Interpretation of the Homogenized Non-penetration Condition

Nevertheless, we can interpret this condition in the mechanical sense also (see Sec.5.5 [12]), like anisotropic Winkler-type condition. That is, for numerical calculations with,

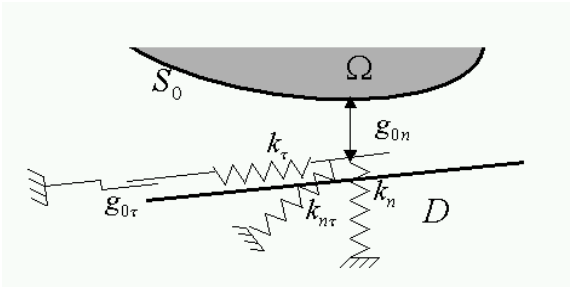

Figure 3: Homogenized anisotropic Winkler-type condition

e.g., ANSYS, the macrocontact can be represented by springs on the interface, which would have different stiffnesses in the normal, tangential and diagonal directions, as it is shown on the Fig.3. Recall here that we started with only normal micro-contact stiffness $k_n^{\varepsilon,\delta} = \frac{1}{\delta} b(\hat{x}, \frac{\hat{x}}{\varepsilon})$. According to Proposition 23 and (25), the limiting from (7) contact integral will be the following:

$$\frac{1}{\delta|T|}\int_{S_0}\int_{S_C} b(\hat{x},\hat{\xi})[\mathbf{u}^{\mathbf{R0},\delta}(x)\cdot n(x,\xi) - g_0(x)]_+ n(x,\xi)\cdot(\mathbf{v}^{\mathbf{R0}}(x) - \mathbf{u}^{\mathbf{R0},\delta}(x))ds_\xi ds. \quad (31)$$

Denote the macro-normal and unit tangential vectors by $\mathbf{n^0}$ and $\hat{\tau}^{\mathbf{0}} = (\tau_{\mathbf{1}}^{\mathbf{0}}, ..., \tau_{\mathbf{n-1}}^{\mathbf{0}})$. Furthermore, let the micro-normal $\mathbf{n}(x,\xi) = \beta_1(\xi)\mathbf{n^0}(x) + \hat{\beta}(\xi)\hat{\tau}^{\mathbf{0}}(x)$, $\hat{\beta} = (\beta_2, ..., \beta_n)$ (recall that **n** coincides also with ξ_1-direction). Then for almost every $x \in S_0$, the normal homogenized stress will be

$$\sigma_n^{0,\delta} = -\frac{1}{\delta|T|}\int_{S_C} b(\hat{x},\hat{\xi})[\beta_1^2(\xi)u_n^{R0,\delta}(x) + \hat{\beta}(\xi)\beta_1(\xi)u_t^{R0,\delta}(x) - \beta_1(\xi)g_0(x)]_+ ds_\xi \quad (32)$$

and the tangential homogenized contact stress $\hat{\sigma}^0_\tau = (\sigma^0_{\tau j})_{j=n-1}$ will be

$$\hat{\sigma}^{0,\delta}_{t_j} = -\frac{1}{\delta|T|}\int_{S_C} b(\hat{x},\hat{\xi})[\beta^2_{j+1}(\xi)u^{R0,\delta}_t(x) + \beta_1(\xi)\beta_{j+1}(\xi)u^{R0,\delta}_n(x) - \beta_{j+1}(\xi)g_0(x)]_+ ds_\xi. \tag{33}$$

The initial gap $\hat{g}(x,\xi)$ related on the microgeometry of the interface as well as the displacement inside of the contact layer are dissapeared in the limit. Nevertheless, the nonlinear function $[\frac{u^\varepsilon_n(x)-u^0_n(x)}{\varepsilon} - \hat{g}(x,\xi)]_+$ related on the non-penetration condition inside the periodicity cell from the contact layer should be preserved by replacing of the full potentially contact surface S_C by S^{real}_C. It means that the integral will be equal to zero at the parts of S_C, which will be not in a contact. That is, in order to calculate the homogenized contact stiffnesses, gap and slider on Fig. 3, we need to know the real contact surface $S^{real}_C \leq S_C$ and integrate over it in equations above. The real contact zone on S_C can be found from the solution of auxiliary periodicity cell problem related to each value of macrostresses $\sigma^0(\hat{x})$, $\hat{x} \in S_0$ (see further Sec. 3.4).

$$\begin{aligned}
k^0_n &= -\frac{1}{|T|}\int_{S^{real}_C(\sigma^0)} k_n(\hat{x},\hat{\xi})\beta^2_1(\xi)ds_\xi, \quad k^0_{t_j} = -\frac{1}{|T|}\int_{S^{real}_C(\sigma^0)} k_n(\hat{x},\hat{\xi})\beta^2_{j+1}(\xi)ds_\xi,\\
k^0_{nt_j} &= -\frac{1}{|T|}\int_{S^{real}_C(\sigma^0)} k_n(\hat{x},\hat{\xi})\beta_1(\xi)\beta_{j+1}(\xi)ds_\xi, \quad j = 1,...,n-1\\
g^0_n &= \left(\frac{1}{|T|}\int_{S^{real}_C(\sigma^0)} k_n(\hat{x},\hat{\xi})\beta_1(\xi)ds_\xi\right) g_0(x),\\
g^0_{t_j} &= \left(\frac{1}{|T|}\int_{S^{real}_C(\sigma^0)} k_n(\hat{x},\hat{\xi})\beta_{j+1}(\xi)ds_\xi\right) g_0(x).
\end{aligned} \tag{34}$$

Let us remark here that the mixed component of the contact stiffness disappear for symmetric micro-cavities. The diagonal and tangential macro-stiffnesses, $k^0_{nt_j}$ and $k^0 t_j$, will implies some tangential drag forces, which can be interpreted as friction forces. The drag forces caused by $k^0_{nt_j}$ can be represented in the form of the Coulomb's friction with the homogenized friction coefficients $\mu^0_j(x) = \frac{k^0_{nt_j}(x)}{k^0_n(x)}$, $j = 1,...,n-1$, while the forces caused by kt_j reason into the homogenized friction tension $G^0_j(x) = |k^0_{t_j}(x)u_{t_j}(x)|$. These definitions can be used for the macro-problem in following numerical computations. We recall at this place the main result of this paper.

Remark 25 *Starting with the frictionless contact micro-problem with a rough interface, we end up with the macro-problem containing friction.*

Let us consider two trivial examples with known contact area.

Example 26 (Plane contact) *With the assumption that all micro-peaks have plane summits, and thus the contact surface is plane, a simple formula is obtained for the homogenised contact stiffness k_n,*

$$k_n(\hat{x}) = \frac{1}{|T|}\int_{S^{\rm real}_{\rm C}} k^\varepsilon(\hat{x},\xi)\, ds_\xi. \tag{35}$$

In particular, it follows that if $k^\varepsilon = \mathrm{const}$ the characteristic dimensions of the periodicity cell is $|T| = L$, then

$$k^0_n = k_n\,|S^{\rm real}_{\rm C}|/L^2. \tag{36}$$

Example 27 (Full contact) *Let we proceed in the $2-$dimensional space, $b = const$, $g_0 = 0$ and $\beta(\xi)$ denote both the unit outer micronormal vector and the angle between this vector and the macronormal. The following table maps the normal, tangential and mixed contact stiffnesses for each geometry from Fig. 2 respectively for the case, when S_C^{real} coincides with S_C.*

$k_n : \frac{b}{\delta\|T\|}$	a_1	$\sum_{i=1}^{2} a_i \cos^2 \beta_i$	$a\pi/2$
$k_t : \frac{b}{\delta\|T\|}$	a_2	$\sum_{i=1}^{2} a_i \sin^2 \beta_i$	$a\pi/2$
$k_{n,t} : \frac{b}{\delta\|T\|}$	0	$a_1 \cos\beta_1 \sin\beta_1 - a_2 \cos\beta_2 \sin\beta_2$	0

Note that, for all symmetric valleys, the contact condition is isotropic, i.e., $(k_{n,t} = 0)$. Therefor, the limiting case leading to the isotropy for the geometry in the middle is $\beta_1 = \beta_2$.
Suppose in the examples further specifications.
(i) Let in the first picture of Fig.2 $a_1 = |T|$, i.e. the valley occupy in the length the whole periodicity cell. Then k_n-macro coincides with the normal micro-contact stiffness k_n^ε. k_t grows with the growing of the deepness a_2 of the valley.
(ii) Let on the figure in the middle $\beta_1 = \beta_2$. If $\beta_1 = \beta_2 = 0$, i.e., there is no micro-valleys, then the macro-normal stiffness k_n coincides again with the micro-contact stiffness b/δ. If we choose the triangular valley of the same deepness as the rectangular valley on the first figure, then, for $\beta_1 = \beta_2 = \frac{\pi}{6}$, k_t for the first and for the second figures will be equal. With the growth of the angle β_1 its sin *as well as the length a_1 grow and hence k_t becomes greater.*
(iii) In order to reach $k_n = k_n^\varepsilon$ for the last figure, we need to choose $a = \frac{2|T|}{\pi}$.
If we choose the semispherical valley of the same deepness as the rectangular on the first picture, i.e, $a^{(3)} = a_2^{(1)}$. Then $k_t^{(3)}$ will be greater than $k_t^{(1)}$ (see the table above).

3.2.3 Homogenization of the Frictional Term

In this subsection we consider the frictional contact integral

$$\int_{S_C^{\varepsilon real}} G_i^\varepsilon(x) |v_{\rm it}^R(x)|\, ds. \tag{37}$$

We let here, $\mathbf{g}^\varepsilon(v(x), x) := G_i^\varepsilon(x)|v^R(x) \cdot \tau_i^\varepsilon(x)|$. Such a function $\mathbf{g}^\varepsilon(\eta, x)$ also satisfies assumptions of Lemma 18 for any constant function u. Applying Lemma 18 we obtain that

Proposition 28 $\mathbf{g}^\varepsilon(v(x), x) := G_i^\varepsilon(x)|v^R(x) \cdot \tau_i^\varepsilon(x)|$ *converges in the sense of (25) to* $\mathbf{g}(v^0(0, \hat{x}), \hat{x}, \xi) := G_i(\hat{x}, \frac{\hat{x}}{\varepsilon})|v^{R0}(x) \cdot \tau_i(x, \xi)|$.

According to Proposition 28 and (25), the limiting from (37) integral will be the following:

$$\frac{1}{|T|} \int_{S_0} \int_{S_C^{real}} G_i(\hat{x}, \hat{\xi}) |\mathbf{v^{R0}}(x) \cdot \tau_i(x, \xi)| ds_\xi ds. \tag{38}$$

Denote

$$\tau_i(x, \xi) = \alpha_1^{(i)}(\xi)\mathbf{n^0} + \sum_{j=1}^{n-1} \alpha_{j+1}^{(i)}(\xi)\tau_{\mathbf{j}}^{\mathbf{0}}(x). \tag{39}$$

Then, we can apply the Hölder inequality

$$\frac{1}{|T|} \int_{S_0} \int_{S_C^{real}} G_i(\hat{x}, \hat{\xi}) |\mathbf{v^{R0}}(x) \cdot \tau_i(x, \xi)| ds_\xi ds \tag{40}$$

$$\leq \frac{1}{|T|} \int_{S_0} \int_{S_C^{real}} G_i(\hat{x}, \hat{\xi}) (|\alpha_1^{(i)}(\xi)||v_n^{R0}(x)| + \sum_{j=1}^{n-1} |\alpha_{j+1}^{(i)}(\xi)||v_{jt}^{R0}(x)|) ds_\xi ds. \tag{41}$$

Thus, for almost every $x \in S_0$, the macro-normal component of the frictional force will be given by

$$G_n^0(\hat{x}) \leq \frac{1}{|T|} \int_{S_C^{real}(\sigma^0)} G_i(\hat{x}, \hat{\xi}) |\alpha_1^{(i)}(\xi)| ds_\xi, \tag{42}$$

and the tangential components by

$$G_{jt}^0(\hat{x}) \leq \frac{1}{|T|} \int_{S_C^{real}(\sigma^0)} G_i(\hat{x}, \hat{\xi}) |\alpha_{j+1}^{(i)}(\xi)| ds_\xi. \tag{43}$$

Thus we can conclude that the micro-normal non-penetration condition contribute to the macro-tangential contact stresses and wise-verse, the micro-friction contribute to the macro-normal contact force (such a fenomena is mentioned in Sec.III.5 [5]).

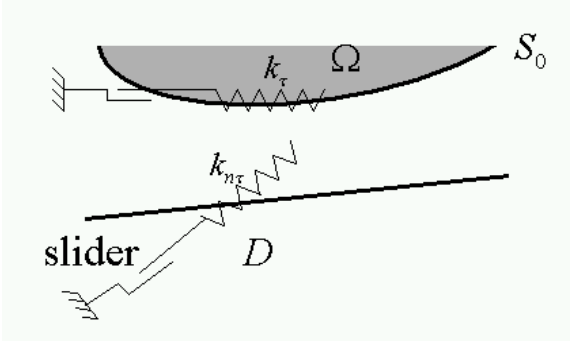

Figure 4: Homogenized friction

$$\begin{aligned}
&|\sigma_{it}^0(x)| < G_{it}^0(\hat{x}), \quad \Rightarrow \quad u_{it}^0 = 0, \quad x \in S_0, \\
&|\sigma_{it}^0| = G_{it}^0(\hat{x}), \quad \Rightarrow \quad \text{there } \exists\ k_\tau \geq 0 \text{ such that } \quad \sigma_{it}^0 = -k_\tau u_{it}^0, \quad x \in S_0, \\
&|\sigma_{it}^0| = G_n^0(\hat{x}), \quad \Rightarrow \quad \text{there } \exists\ k_{n\tau} \text{ such that } \quad \sigma_{it}^0 = k_{n\tau} u_{\mathrm{n}}^0, \quad x \in S_0,
\end{aligned}$$

Recalling the fact, that G_n^0, G_{it}^0 depend on the micro-contact surface, which is further depending on the macrostresses in the contact layer, i.e., on the macrointerface, the macro-contact friction condition can be determined iteratively as the following:

$$\begin{aligned}
&|\sigma_{it}^{0n+1}(x)| < G_{it}^0(\sigma^{\mathbf{0}^n}, \hat{x}), \quad \Rightarrow \quad u_{it}^{0n+1} = 0, \quad x \in S_0, \\
&|\sigma_{it}^{0n+1}| = G_{it}^0(\sigma^{\mathbf{0}^n}, \hat{x}), \quad \Rightarrow \quad \text{there } \exists\ k_\tau \geq 0 \text{ such that } \quad \sigma_{it}^{0n+1} = -k_\tau u_{it}^{0n+1}, \quad x \in S_0, \\
&|\sigma_{it}^{0n+1}| = G_n^0(\sigma^{\mathbf{0}^n}, \hat{x}), \quad \Rightarrow \quad \text{there } \exists\ k_{n\tau} \text{ such that } \quad \sigma_{it}^{0n+1} = k_{n\tau} u_{\mathrm{n}}^{0n+1}, \quad x \in S_0,
\end{aligned}$$

where $n = 1, 2, ...$ are iteration steps. This scheme should be used for the numerical algorithm. The only step for determining the real contact surface S_C^{real} in the periodicity cell in dependence on $\sigma^{\mathbf{0}}$ is missing. This step will be demonstrated in Sectoins 3.4, 3.5.

Let us continue with our problem.

3.3 Homogenized Problem

The results of this subsection were obtained by G. Yosifian in 2000 and became known to the author of this paper through the private communication.

Proposition 29 *For each fixed small $\delta > 0$, functional $I^{\varepsilon,\delta}(u^\varepsilon)$ defined by (9) converges to $I^0(u^0)$ defined by*

$$I^0(v^0) = \frac{1}{2}\int_\Omega a_{ijkl}\frac{\partial v_k^0(x)}{\partial x_l}\frac{\partial v_i^0(x)}{\partial x_j}\,dx + \frac{1}{|T|}\int_{S_0} G_{in}^0(\hat{x})|v_{\rm in}^0(0,\hat{x})|\,d\hat{x}$$
$$+ \frac{1}{|T|}\int_{S_0} G_{it}^0(\hat{x})|v_{\rm it}^0(0,\hat{x})|\,d\hat{x}$$
$$- \int_\Omega f_i(x)v_i^0(x)dx - \int_{\partial\Omega_N} t_i(x)v_i^0(x)ds, \tag{44}$$

for any $v_i^0 \in \mathcal{K} := \{\mathbf{v^0} \in (H_0^1(\Omega\cup D, \partial\Omega_u\cup\partial D_u))^n |\ \mathbf{v^0}(x)\cdot n(x,\xi) \le g_0(x),$ a.e. in $\xi \in S_C,$ a.e. on $S_0\}$. Furthermore, the weak limit u^0 of the sequence u^ε, which is minimizer of (9), is a minimizer of (44).

Proof:
According to Prop. 6, the solution of equation (6) is uniformly bounded in $H^1(\Omega\cup D)$ and hence has a weak convergent subsequence. We pass to the limit inf (or $\Gamma-\lim$ see Def.1.1 in A.1.1 [9]) as $\varepsilon\to 0$ in equation (6) in accordance with Propositions 17, 23 and 28. We obtain for any $v_i^0 \in \mathcal{K} := \{\mathbf{v^0} \in (H_0^1(\Omega\cup D, \partial\Omega_u\cup\partial D_u))^n |\ \mathbf{v^0}(x)\cdot n(x,\xi) \le g_0(x),$ a.e. in $\xi\in S_C,$ a.e. on $S_0\}$ the following relation:

$$\int_\Omega a_{ijkl}\frac{\partial u_k^0(x)}{\partial x_l}\frac{\partial (v_i^0(x)-u_i^0(x))}{\partial x_j}\,dx$$
$$+\frac{1}{|T|}\int_{S_0} G_{in}^0(\hat{x})(|v_{\rm in}^0(0,\hat{x})| - |u_{\rm in}^0(0,\hat{x})|)\,d\hat{x}$$
$$+\frac{1}{|T|}\int_{S_0} G_{it}^0(\hat{x})(|v_{\rm it}^0(0,\hat{x})| - |u_{\rm it}^0(0,\hat{x})|)\,d\hat{x}$$
$$\ge \int_\Omega f_i(x)(v_i^0(x)-u_i^0(x))dx + \int_{\partial\Omega_N} t_i(x)(v_i^0(x)-u_i^0(x))ds, \tag{45}$$

where $|T|$ stands for the measure of the domain T.
Functional (44) is obtained from (45) on the same way as (9) from (6). Since functional (9) converges to (44) in the sense of Γ-convergence (see [9]), owing to Theorem 1.3, A1.1 [9], the minimizers of (9) converge to those of (44), i.e., the weak limit u^0 of the sequence u^ε, which is minimizer of (9), is a minimizer of (44).

To the variational formulation (45) there corresponds the *homogenized problem* in the strong formulation

$$\frac{\partial\sigma_{ij}^0(x)}{\partial x_j} = f_i(x), \quad \sigma_{ij}^0(x) = a_{ijkl}\frac{\partial u_k^0(x)}{\partial x_l}, \qquad x\in\Omega\cup D, \tag{46}$$
$$\sigma_{\rm n}^0(x)\le 0,\ \ [u^0(x)\cdot n(x,\xi)]\le g_0(x),\ \ \sigma_{\rm n}^0(x)[u^0(x)\cdot n(x,\xi)-g_0(x)] = 0$$
$$\text{for a.a. } \xi\in S_C,\ \ x\in S_0,$$
$$|\sigma_{\rm it}^0(x)| < G_{it}^0(\hat{x}), \qquad \Rightarrow \qquad u_{\rm it}^0 = 0, \qquad x\in S_0, \tag{47}$$
$$|\sigma_{\rm it}^0| = G_{it}^0(\hat{x}), \qquad \Rightarrow \qquad \text{there } \exists\ k_\tau\ge 0 \text{ such that} \qquad \sigma_{\rm it}^0 = -k_\tau u_{\rm it}^0, \qquad x\in S_0,$$
$$|\sigma_{\rm it}^0| = G_n^0(\hat{x}), \qquad \Rightarrow \qquad \text{there } \exists\ k_{n\tau} \text{ such that} \qquad \sigma_{\rm it}^0 = k_{n\tau}u_{\rm n}^0, \qquad x\in S_0,$$
$$\sigma_{ij}^0(x)n_j(x) = t_i(x), \quad x\in\partial\Omega_{\rm N}\cup D_{\rm N}; \qquad u_i^0(x) = 0, \quad x\in\partial\Omega_u\cup D_u. \tag{48}$$

Now, we need to find a contact surface $S_C^{real}(u^0)$ using the micro-contact information in the interface layer.

3.4 Auxiliary Problem in the Interface Layer

This subsection can be considered as the main result of this work.
Let us first consider the formal asymptotic expansion, which should give the strong formulation of the auxiliary problem in the interface layer, and then try to choose some appropriate test function v for (6), which will yield the corresponding variational statement in the limit.

3.4.1 Formal Asymptotic Expansion and Strong Interpretation of the Auxiliary Problem

We will represent the unknown microsolution $u_i^\varepsilon(x)$ in the form of an asymptotic expansion. Let εT be the period of the structure at the interface. According to [10],

$$u_i^\varepsilon(x) = u_i^0(x) + \varepsilon u_i^1(x,\xi) + O(\varepsilon^2),$$

where $\xi = x/\varepsilon$, $x \in \Omega \cup D$, $\xi \in Y_1 \cap \varepsilon^{-1}(\Omega^\varepsilon \cup D^\varepsilon)$. If we put this expansion into the strong formulation of our microproblem (1)-(3) and take all partial derivatives with respect to the following rule

$$\frac{\partial u^\varepsilon(x)}{\partial x} = \frac{\partial u(x,\xi)}{\partial x} + \frac{1}{\varepsilon}\frac{\partial u(x,\xi)}{\partial \xi},$$

we verify that $(u_i^0)_n$, $u_i^0 \in H^1(\Omega \cup D)$, is the solution of macroproblem (46) obtained after replacing the contact layer by the homogenized contact condition (47), $(u_i^1)_{n\times n}$, $u_i^1 \in L^2(S_0^{real}, H^1_{per}(Y_1))$, is the periodic in $\hat{\xi}$ solution of the auxiliary cell problems in cells containing in the real macro-contact surface $S_0^{real} := \{x \in S_0 |\ \mathbf{u}^0(x)\cdot\mathbf{n}(x,\xi) = g_0(x)\}$

$$\frac{\partial}{\partial \xi_j}\left[a_{ijkl}\frac{\partial u_k^1(x,\xi)}{\partial \xi_l}\right] = -\frac{\partial \sigma_{ij}^0(x)}{\partial \xi_j}(=0), \qquad \xi \in Y_1, \tag{49}$$

with modified Signorini's and friction contact conditions

$$\begin{aligned}
&\sigma_{\rm n}^1(x,\xi) \equiv a_{ijkl}(x)\frac{\partial u_k^1(x,\xi)}{\partial \xi_l} n_j(x,\xi) n_i(x,\xi) \le -\sigma_{ij}^0(x) n_j(x,\xi) n_i(x,\xi),\\
&\quad [u_i^1(x,\xi)\cdot n_i(x,\xi)] \le \bar{g}(\xi),\\
&(\sigma_{\rm n}^1(x,\xi) + \sigma_{ij}^0(x) n_j(x,\xi) n_i(x,\xi))[u_i^1(x,\xi)\cdot n_i(x,\xi) - \bar{g}(\xi)] = 0 \qquad \xi \in S_{\rm C},\\
&|\sigma_{\rm it}^1(x,\xi)| \equiv |a_{ijkl}\frac{\partial u_k^1(x,\xi)}{\partial \xi_l} n_j(x,\xi) - \sigma_{\rm n}^1 n_i(x,\xi)| < G(\hat{x},\hat{\xi}),\\
&\qquad\qquad \Rightarrow \qquad u_{\rm it}^0 = 0, \qquad \xi \in S_{\rm C},
\end{aligned} \tag{50}$$

$$|\sigma_{\rm it}^1(x,\xi)| = G(\hat{x},\hat{\xi}), \ \Rightarrow \ \exists\, \lambda \ge 0\colon \qquad u_{\rm it}^1 = -\lambda \sigma_{\rm it}(u^1), \qquad \xi \in S_{\rm C},$$

and the boundary condition on $\xi_1 = \pm\infty$

$$\sigma_{i1}^1(x,\xi) = (-\sigma_{ij}^0(x) n_j(x,\xi) + t_i(x))|_{x\in\partial\Omega_N^\varepsilon \cup \partial D_N^\varepsilon} \equiv 0,$$

for such x that $Y_1 \cap \varepsilon^{-1}(\partial\Omega_N^\varepsilon \cup \partial D_N^\varepsilon)$ is non-empty, and

$$u_i^1(x,\xi) = 0, \ \xi_1 = \pm\infty \qquad \text{otherwise}. \tag{51}$$

Remark 30 *All the constrains and equalities of the system above were obtained by collection of terms of the power ε^0 and only the non-penetration condition $[u^1(x,\xi)\cdot n(x,\xi)] \le \bar{g}(\xi)$ and the Dirichlet condition on $\xi_1 = \infty$ were obtained from the collection of terms with ε^1.*

Note here that the term $\sigma^0(x)$ is depending only on the macro-variable x and is independent of ξ, i.e., constant on S_C. It can be interpreted as a known fictitious anisotropic temperature or shrinkage stress. Furthermore, condition (50) claims that on both of contacting surfaces on each part non-being in the contact some pressure is applied, which is known from the macro-problem and constant in the cell. This pressure reasons also the frictional force on the contact surfaces.
From this problem and solvability solution to it, the micro-contact area can be determined.

3.4.2 Two-scale Convergence and Variational Formulation of the Auxiliary Problem

The following Lemma is an auxiliary instrument for the proof of the central proposition of this section.

Lemma 31 *Let $\Omega' \subset \Omega$ and $\mathbf{g}^\varepsilon(\eta, y, \xi)$ defined on $\mathbb{R}^n \times \bar{\Omega}' \times S_C$ satisfies the inequalities:*

$$\sup_{\xi \in S_C} |\mathbf{g}^\varepsilon(\eta, y_1, \xi) - \mathbf{g}^\varepsilon(\eta, y_2, \xi)| \leq \mu(1 + |\eta|)|y^1 - y^2|, \qquad \forall y^1, y^2 \in \Omega', \eta \in \mathbb{R}^n,$$

$$\sup_{y \in \Omega\ \xi \in S_C} |\mathbf{g}^\varepsilon(\eta^1, y, \xi) - \mathbf{g}^\varepsilon(\eta^2, y, \xi)| \leq \mu|\eta^1 - \eta^2|, \qquad \forall \eta^1, \eta^2 \in \mathbb{R}^n,$$

where μ is a positive constant, and has almost everywhere in Ω' the representation: $\mathbf{g}^\varepsilon(\eta, x) = \mathbf{g}(\eta, x, \varepsilon^{-1}x)$. Then for any sequence $u^\varepsilon \in (H^1(\Omega))^n$ such that, up to a subsequence, u^ε two-scale converges to $u^0(x)$ and ∇u^ε two-scale converges to $\nabla u^0(x) + \nabla_\xi u^1(x, \xi)$ as $\varepsilon \to 0$, $u^0 \in H^1(\Omega)$ $u^1 \in L^2(\Omega, H^1_{per}(Y))$, and for any admissible test function $v^1 \in \mathcal{D}(\Omega, C^\infty_{per}(Y))$, we have the convergence:

$$\varepsilon \int_{S^\varepsilon_C \cap \Omega'} \mathbf{g}^\varepsilon(v^1(x, \frac{x}{\varepsilon}), x) ds \to \frac{1}{|Y|} \int_{\Omega'} \int_{S_C} \mathbf{g}(v^1(x, \xi), x, \xi) ds_\xi dx, \tag{52}$$

and

$$\varepsilon \int_{S^\varepsilon_C \cap \Omega'} \mathbf{g}^\varepsilon(u^\varepsilon(x), x) v^1(x, \frac{x}{\varepsilon}) ds \to \frac{1}{|Y|} \int_{\Omega'} \int_{S_C} \mathbf{g}(u^0(x, \xi), x, \xi) v^1(x, \xi) ds_\xi dx, \tag{53}$$

Proof:
The idea is the same as in the proof of Lemma 20.
Let us denote $\phi(x, \frac{x}{\varepsilon}) := g(v^1(x, \frac{x}{\varepsilon}), x, \frac{x}{\varepsilon})$. Owing to the first inequality required from $\mathbf{g}$, $\phi \in (L^2(\Omega, H^1_{per}(Y)))^n$, hence its trace is in $(L^2(\Omega, L^2(S_C)))^n$. According to Lemma 15, $\phi(x, \frac{x}{\varepsilon})$ satisfies

$$\varepsilon \int_{S^\varepsilon_C \cap \Omega'} \phi(x, \frac{x}{\varepsilon}) v^1(x, \frac{x}{\varepsilon}) ds \to \frac{1}{|Y|} \int_{\Omega'} \int_{S_C} \phi(x, \xi) v^1(x, \xi) ds_\xi dx, \tag{54}$$

for any admissible test function $v^1 \in L^2(\Omega, H^1_{per}(Y))$. Hence, (52) holds true.
Let us rewrite the left-hand side of (53) in the following way:

$$\begin{aligned} &\varepsilon \int_{S^\varepsilon_C \cap \Omega'} \mathbf{g}^\varepsilon(u^\varepsilon(x), x) v^1(x, \frac{x}{\varepsilon}) ds = \varepsilon \int_{S^\varepsilon_C \cap \Omega'} \mathbf{g}^\varepsilon(u^0(x), x) v^1(x, \frac{x}{\varepsilon}) ds \\ &+\varepsilon \int_{S^\varepsilon_C \cap \Omega'} (\mathbf{g}^\varepsilon(u^\varepsilon(x), x) - \mathbf{g}^\varepsilon(u^0(x), x)) v^1(x, \frac{x}{\varepsilon}) ds \end{aligned} \tag{55}$$

Applying the second required from $\mathbf{g}$ inequality, Lemmma 14 and the property v as a test function claimed by Lemma 10, we can estimate the last term as the following:

$$\varepsilon \int_{S_C^\varepsilon \cap \Omega'} (\mathbf{g}^\varepsilon(u^\varepsilon(x),x) - \mathbf{g}^\varepsilon(u^\varepsilon(x),x)) v^1(x,\frac{x}{\varepsilon}) ds \le \varepsilon\mu \int_{S_C^\varepsilon \cap \Omega'} |u^\varepsilon(x) - u^0(x)| v^1(x,\frac{x}{\varepsilon}) ds$$
$$\le \varepsilon\mu ||u^\varepsilon(x) - u^0(x)||_{L^2(S_C^\varepsilon \cap \Omega')} ||v^1||_{L^2(S_C^\varepsilon \cap \Omega')} \le \varepsilon\mu c_3^2 \left(\varepsilon^{-1/2} ||u^\varepsilon(x) - u^0(x)||_{L^2(\Omega')}\right.$$
$$\left. + \varepsilon^{1/2} ||\nabla_x u^\varepsilon(x) - \nabla_x u^0(x))||_{L^2(\Omega')}\right) \left(\varepsilon^{-1/2} ||v^1(x,\frac{x}{\varepsilon})||_{L^2(\Omega')} + \varepsilon^{1/2} ||\nabla_x v^1(x,\frac{x}{\varepsilon})||_{L^2(\Omega')}\right)$$
$$= \mu c_4 \left(||u^\varepsilon(x) - u^0(x)||_{L^2(\Omega')} + \varepsilon ||\nabla_x u^\varepsilon(x) - \nabla_x u^0(x))||_{L^2(\Omega')}\right)$$
$$\cdot \left(||v^1(x,\frac{x}{\varepsilon})||_{L^2(\Omega')} + \varepsilon ||\nabla_x v^1(x,\frac{x}{\varepsilon})||_{L^2(\Omega')}\right) \tag{56}$$

Since u^0 is independing of the fast variable and belongs to $(H^1(\Omega))^n$, it is smooth enough for (22) to fulfill. Thus the first term of the last expression tends to 0 as $\varepsilon \to 0$.
Owing to Lemma 10, since $u^1 \in (L^2(\Omega, H^1_{per}(Y)))^n$, it is "admissible" test function, and, hence, the statement of Theorem 13 is valid. It means that

$$\lim_{\varepsilon\to 0} ||\nabla_x u^\varepsilon(x) - \nabla_x u^0(x))||_{L^2(\Omega')} = ||\nabla_\xi u^1(x,\xi)||_{L^2(\Omega'\times Y)},$$

which is bounded.
Owing to the fact that v^1 is also "admissible",

$$\lim_{\varepsilon\to 0} ||v^1(x,\frac{x}{\varepsilon})||_{L^2(\Omega')} = ||v^1(x,\xi)||_{L^2(\Omega'\times Y)}.$$

Furthermore,

$$||\nabla v^1(x,\frac{x}{\varepsilon})||_{L^2(\Omega')} \le ||\nabla_x v^1(x,\xi)||||_{L^2(\Omega'\times Y)} + \varepsilon^{-1/2} ||\nabla_\xi v^1(x,\xi)||_{L^2(\Omega'\times Y)}$$

and, hence, $\lim_{\varepsilon\to 0} \varepsilon ||\nabla v^1(x,\frac{x}{\varepsilon})||_{L^2(\Omega')} = 0$.
Thus, the $\lim_{\varepsilon\to 0}$ of the last term in (55) is zero.
Denote again $\phi(x,\frac{x}{\varepsilon}) := \mathbf{g}(u^0(x),x,\frac{x}{\varepsilon}) v^1(x,\frac{x}{\varepsilon})$ and repeat the first part of the proof.

Proposition 32 *The contact surface $S_C^{real}(u^0)$ can be found from the solution of the auxiliary variational contact problem on the periodicity cells contained in the interface layer:*

$$\int_Y a_{ijkl}(x) \frac{\partial u_k^1(x,\xi)}{\partial \xi_l} \frac{\partial (v_i^1(x,\xi) - u_i^1(x,\xi))}{\partial \xi_j} d\xi \tag{57}$$
$$+ \int_{S_C} G_i(\hat{x},\hat{\xi}) |\tau_{ij}(x,\xi)| (|v_j^{R1}(x,\xi)| - |u_j^{R1,\delta}(x,\xi)|)\, ds_\xi$$
$$\ge -\sigma_{ij}^0(x) \int_{S_C} \left(1 - H(u_i^{R1}(x,\xi) n_i(x,\xi) - \bar{g}_i(x,\xi))\right) n_j(x,\xi) (v_i^1(x,\xi) - u_i^1(x,\xi))\, dS_\xi$$

for a.a. $x \in S_0^{real} = \{x \in S_0,\ \mathbf{u}^0(x)\cdot\mathbf{n}(x,\xi) = g_0(x)\}$ and any $v^1 \in \mathcal{K}^1$, where $\mathcal{K}^1 := \{v^1 \in (L^2(S_0^{real}, (H^1_{per}(Y_1))^n |\ v_n^{R1}(x,\xi) \le \bar{g}(\xi)$ for $\xi \in S_C$ and a.a. $x \in S_0^{real}\}$.

Proof:
Let us consider the variational inequality (11) now. We define a non-negative variational form

$$J(u^{\varepsilon,\delta}, v) := \int_{\Omega^\varepsilon \cup D^\varepsilon} a_{ijkl}(x) \frac{\partial u_k^{\varepsilon,\delta}(x)}{\partial x_l} \frac{\partial (v_i(x) - u_i^{\varepsilon,\delta}(x))}{\partial x_j} dx$$

$$+\int_{S_{\rm C}^\varepsilon} b^{\varepsilon,\delta}(x)[u_{\rm n}^{R\varepsilon,\delta}(x)-g_0(x)-\varepsilon\bar g(\frac{x}{\varepsilon})]_+(v_{\rm n}^R-\hat u_{\rm n}^{R\varepsilon,\delta})\,ds$$
$$+\int_{S_{\rm C}^\varepsilon} G_i^\varepsilon(x)(|v_{i\rm t}^R(x)|-|u_{i\rm t}^{R\varepsilon,\delta}(x)|)\,ds-\int_{\Omega^\varepsilon\cup D^\varepsilon} f_i(x)(v_i(x)-u_i^{\varepsilon,\delta}(x))dx \quad (58)$$
$$-\int_{\partial\Omega_N^\varepsilon\cup\partial D_N^\varepsilon} t_i(x)(v_i(x)-u_i^{\varepsilon,\delta}(x))ds,$$

and consider $lim_{\varepsilon\to 0}J(\hat u^\varepsilon,v^\varepsilon)\geq 0$ with a test-function $v^\varepsilon(x)=v^0(x)+\varepsilon v^1(x,\frac{x}{\varepsilon})$, where $v^0(x)\in(H_0^1(\Omega\cup D,\partial\Omega\cup\partial D))^n$ and $v^1\in(H^1(\Omega\cup D),H^1_{per}(Y))^n$. Recall that $\tilde g_j^\varepsilon\in H^1(\Omega^\varepsilon\cup D^\varepsilon)$, such that $\{\tilde g_i^\varepsilon|_{\partial\Omega_u^\varepsilon\cup\partial D_u^\varepsilon}=g_{i0},\ \tilde{\mathbf g}^\varepsilon\cdot\mathbf n|_{S_C^{\varepsilon+}}-\tilde{\mathbf g}^\varepsilon\cdot\mathbf n|_{S_C^{\varepsilon-}}=g^\varepsilon;$ $\tilde{\mathbf g}^\varepsilon\cdot\tau|_{S_C^{\varepsilon+}}-\tilde{\mathbf g}^\varepsilon\cdot\tau|_{S_C^{\varepsilon-}}=0\}$, and $g^\varepsilon(\hat x)=g_0(\hat x)+\varepsilon\bar g(\hat x,\frac{\hat x}{\varepsilon})$.
Let us make some auxiliary considerations for the convergence of each term of the variational form.
Owing to Theorem 11, definition of the two-scale convergence and considerations used in The. 3.2 [1],

$$\lim_{\varepsilon\to 0}\int_{\Omega^\varepsilon\cup D^\varepsilon} a_{ijkl}(x)\frac{\partial\hat u_k^\varepsilon(x)}{\partial x_l}\frac{\partial(v_i(x)-\hat u_i^{\varepsilon,\delta}(x))}{\partial x_j}\,dx \quad (59)$$
$$=\int_{\Omega\cup D}\frac{1}{|Y|}\int_Y a_{ijkl}(x)\left(\frac{\partial\hat u_k^0(x)}{\partial x_l}+\frac{\partial\hat u_k^1(x,\xi)}{\partial\xi_l}\right)$$
$$\cdot\left(\frac{\partial v_i^0(x)-\hat u_i^{0,\delta}(x))}{\partial x_j}+\frac{\partial(v_i^1(x,\xi)-\hat u_i^{1,\delta}(x,\xi))}{\partial\xi_j}\right)d\xi\,dx,$$

for the fourth and fifth terms:

$$\lim_{\varepsilon\to 0}\int_{\Omega^\varepsilon\cup D^\varepsilon}\left(f_i(x)(v_i(x)-\hat u_i^{\varepsilon,\delta}(x))\right)dx+\int_{\partial\Omega_N^\varepsilon\cup\partial D_N^\varepsilon} t_i(x)(v_i(x)-\hat u_i^{\varepsilon,\delta}(x))ds \quad (60)$$
$$=\int_{\Omega\cup D}\left(f_i(x)(v_i^0(x)-\hat u_i^{0,\delta}(x))\right)dx+\int_{\partial\Omega_N\cup\partial D_N} t_i(x)(v_i^0(x)-\hat u_i^{0,\delta}(x))ds.$$

We take $v^0(x)=\hat u^{0,\delta}(x)$, where $\hat u^{0,\delta}(x)\in(H_0^1(\Omega\cup D,\partial\Omega\cup\partial D))^n$ is the homogenized solution and weak and two-scale limit of $\hat u^{\varepsilon,\delta}$.
Since $v^0(x)=\hat u^{0,\delta}(x)$, the third and fifth terms of the variational form will disappear in $lim_{\varepsilon\to 0}J(\hat u^\varepsilon,v^\varepsilon)$.
Owing to Lemma 31,

$$\lim_{\varepsilon\to 0}\int_{S_{\rm C}^\varepsilon} b^{\varepsilon,\delta}(x)[u_{\rm n}^{R\varepsilon,\delta}(x)-g_0(x)-\varepsilon\bar g(\frac{x}{\varepsilon})]_+(u_{\rm n}^{R0}(x)+\varepsilon v_{\rm n}^{R1}(x,\frac{x}{\varepsilon})-u_{\rm n}^{R\varepsilon,\delta}(x))\,ds \quad (61)$$
$$=\int_\Omega\frac{1}{\delta|Y|}\int_{S_C} b(x,\xi)[u_i^{R0,\delta}(x)n_i(x,\xi)-g_{0i}(x)]_+n_j(x,\xi)(v_j^{R1}(x,\xi)-u_j^{R1,\delta}(x))ds_\xi dx,$$

$$\lim_{\varepsilon\to 0}\int_{S_{\rm C}^\varepsilon} G_i^\varepsilon(x)|\varepsilon v_{\rm t}^{R1}(x,\frac{x}{\varepsilon})|\,ds=\int_\Omega\frac{1}{|Y|}\int_{S_{\rm C}} G_i(x,\xi)|\tau_{ij}(x,\xi)v_j^{R1}(x,\xi)|\,ds_\xi \quad (62)$$

We require further v^1 to be periodic in $\hat\xi$ and compactly supported in x in $\Pi^\varepsilon\cup S_0^{real}$, with the strip $\Pi^\varepsilon=(\Omega^\varepsilon\cup D^\varepsilon)\cap\{x:0<|x_1|<\frac{Y}{2}\varepsilon\}$ and $S_0^{real}=\{x\in S_0,\ \mathbf u^0(x)\cdot\mathbf n(x,\xi)=g_0(x)\}$, and, additionally, $v_n^{R1}(x,\xi)\leq\bar g(\xi)$ for $\xi\in S_C$ almost everywhere on S_0. The last requirement, of the non-penetration on S_C, was guessed owing to Remark 30. We required the fulfilling the macro-contact in order for consideration of the test function v^1 from the contact layer to have sense. Since, we consider only the macro-contact, the

right-hend side of (61) disappear.
Since u^1, v^1, are compactly supported in x in the strip $\Pi^\varepsilon = (\Omega^\varepsilon \cup D^\varepsilon) \cap \{x : 0 < |x_1| < \frac{Y}{2}\varepsilon\}$ and vanish in the rest of domains $\Omega \cup D$, right-hand sides of (59), (61) and (62) are of the order ε with respect to the outer integration.
Let us come over to the next limit $lim_{\varepsilon\to 0}\frac{J^0(u^0+\varepsilon u^1, u^0+\varepsilon v^1)}{\varepsilon}$.
Since, $v_i^1(x,\xi)$ is arbitrary w.r.t. x in the $\varepsilon-$ surrounding of S_0, the limiting variational inequality will be

$$\int_Y a_{ijkl}(x)\left(\frac{\partial u_k^1(x,\xi)}{\partial \xi_l} + \frac{\partial u_k^0(x)}{\partial x_l}\right)\frac{\partial (v_i^1(x,\xi) - u_i^1(x,\xi))}{\partial \xi_j}\, d\xi \tag{63}$$
$$+ \int_{S_C} G_i(\hat{x},\hat{\xi})|\tau_{ij}(x,\xi)|(|v_j^{R1}(x,\xi)| - |u_j^{R1,\delta}(x,\xi)|)\, ds_\xi \geq 0$$

for a.a. $x \in S_0^{real}$. $v^1 \in \mathcal{K}^1$, where $\mathcal{K}^1 := \{v^1 \in (H^{-1/2}(S_0^{real}, (H^1_{per}(Y_1))^n |\ v_n^{R1}(x,\xi) \leq \bar{g}(\xi)$ for $\xi \in S_C$ and a.a. $x \in S_0^{real}\}$

Our next task is to interpret the variational cell-problem (63) in terms of applied loads and constrains, i.e., come over to its strong formulation. For this reason, let us modify (63) using partial integration.
First, we recall that v^1, u^1 are periodic in $\hat{\xi}$ functions and vanish as $\xi_1 \to \pm\infty$. Then,

$$a_{ijkl}(x)\frac{\partial u_k^0(x)}{\partial x_l}\frac{1}{|Y|}\int_Y \frac{\partial (v_i^1(x,\xi) - u_i^1(x,\xi))}{\partial \xi_j}\, d\xi \tag{64}$$
$$= \sigma_{ij}^0(x)\frac{1}{|Y|}\int_{S_C} H(u_i^{R1}(x,\xi)n_i(x,\xi) - \bar{g}_i(x,\xi))n(x,\xi)(v_i^1(x,\xi) - u_i^1(x,\xi))\, dS_\xi$$

By going on with the partial integration, we can rewrite (63) as the following:

$$\int_Y a_{ijkl}(x)\frac{\partial u_k^1(x,\xi)}{\partial \xi_l}\frac{\partial (v_i^1(x,\xi) - u_i^1(x,\xi))}{\partial \xi_j}\, d\xi$$
$$+\frac{1}{\delta}\int_{S_C} b(\hat{x},\hat{\xi})[u_i^{R1}(x,\xi)n_i(x,\xi) - \bar{g}_i(x,\xi)]_+ n_j(x,\xi)(v_j^{R1}(x) - u_j^{R1}(x))ds_\xi \tag{65}$$
$$+ \int_{S_C} G_i(\hat{x},\hat{\xi})|\tau_{ij}(x,\xi)|(|v_j^{R1}(x,\xi)| - |u_j^{R1,\delta}(x,\xi)|)\, ds_\xi$$
$$-\sigma_{ij}^0(x)\int_{S_C} H(u_i^{R1}(x,\xi)n_i(x,\xi) - \bar{g}_i(x,\xi))n(x,\xi)(v_i^1(x,\xi) - u_i^1(x,\xi))\, dS_\xi \geq 0$$

for a.a. $x \in S_0^{real}$ and any $v^1 \in (H^{-1/2}(S_0^{real}), H^1_{per}(Y_1)^n)$.

3.5 Two-scale Algorithm for the Solution of the Contact Problem

The following algorithm needs to be performed for the solution of the complete problem:
(i) In the first step we assume some fixed contact surfaces for the auxiliary cell problem, related to the micro-roughness geometry. We define this zero-approximation by $S_{C(0)}$;
(ii) This contact surface should be substituted into formulas (34) and the zero-approximation to the macro-contact stiffnesses and initial gaps can be found;
(iii) This macro-contact stiffnesses as well as the contact gaps should be substituted in the homogenized problem (46)-(48);
(iv) Solving the homogenized problem (46)-(48) by the Finite element method (FEM), we will find the macro-stresses $\sigma_{(1)}^0$ and put them as external loads in the auxiliary cell-problem (49)-(51);

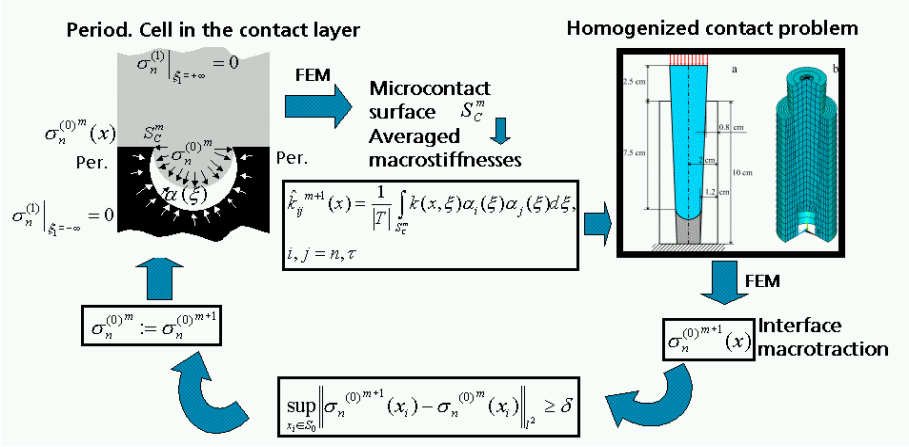

Figure 5: Two-scale algorithm for the contact problem

(v) Then, the auxiliary cell-problem for u^1 should be solved numerically by the FEM. The unknown parts of the contact surface S_C related to the $\sigma^0_{(1)}$ should be found during the solution;
(vi) We will repeat steps (ii)-(vi) until a certain accuracy of the convergence will be reached, i.e. $\sup_{x_i\in\Omega}||\sigma^0_n(x_i)-\sigma^0_{n-1}(x_i)||_{l^2}<\delta$.

4 Linear Problem. Numerical Example.

In this section we consider a simplified problem, where the micro-contact roughness has a plane base, and suppose the contact surface known in order to reduce the problem to a linear one. Furthermore, we approximately assume that the normals to the micro- and macro-contact surfaces coincide.
Let us breafly repeat all considerations of this paper for this case on the formal way.

4.1 Formal asymptotic expansion

We write out the equilibrium equations and constitutive elastic relations with contact and boundary conditions:

$$\frac{\partial\sigma^\varepsilon_{ij}(x)}{\partial x_j}=f_i(x),\quad \sigma^\varepsilon_{ij}(x)=a_{ijkl}\frac{\partial u^\varepsilon_k(x)}{\partial x_l},\qquad x\in\Omega^\varepsilon, \tag{66}$$

$$\sigma^\varepsilon_{\rm n}(x)=k_n\left(\hat{x},\frac{x}{\varepsilon}\right)[u^\varepsilon_{\rm n}(x)],\quad \sigma^\varepsilon_{\rm it}(x)=\mu\sigma^\varepsilon_{\rm n}(x)\frac{u^\varepsilon_{\rm it}}{|u^\varepsilon|},\qquad x\in S^\varepsilon_{\rm C}, \tag{67}$$

$$\sigma^\varepsilon_{ij}n_j(x)=0,\quad x\in S^\varepsilon_{\rm N}\cup\partial\Omega^\varepsilon_{\rm N};\qquad u^\varepsilon_i(x)=0,\quad x\in\partial\Omega^\varepsilon_u. \tag{68}$$

Here k_n means the normal contact stiffness and μ is the friction coefficient ($\mu=0$ in the case of pure sliding).
The homogenized problem in the strong formulation is

$$\frac{\partial\sigma^0_{ij}(x)}{\partial x_j}=f_i(x),\quad \sigma^0_{ij}(x)=a_{ijkl}\frac{\partial u^0_k(x)}{\partial x_l},\qquad x\in\Omega, \tag{69}$$

$$\sigma^0_{\rm n}(x)=k^0_n(\hat{x})[u^0_{\rm n}(x)],\quad \sigma^0_{\rm it}(x)=\mu\sigma^0_{\rm n}(x)\frac{u^0_{\rm it}}{|u^0|},\qquad x\in S_0, \tag{70}$$

$$\sigma^0_{ij}(x)n_j(x)=0,\quad x\in\partial\Omega_{\rm N};\qquad u^0_i(x)=0,\quad x\in\partial\Omega_u, \tag{71}$$

where the homogenized normal contact stiffness is $k_n^0(\hat{x}) = \frac{1}{|T|}\int_{S_C} k_n(\hat{x},\xi)\,ds_\xi$.
Anfortunately, the macro-problem looses the information about mostly stressed regions situated in the boundary layer. Thus, we need to calculate microstresses, which will serve to identify fracture occurrence.
Let εY be the period of the structure at the interface. We look for a microsolution $u_i^\varepsilon(x)$ in the form of an asymptotic expansion [10]:

$$u_i^\varepsilon(x) = \begin{cases} u_i^0(x) & \text{if } x \in \Omega, \\ u_i^0(x) + \varepsilon\Theta_{ip}(\xi)u_p^0(x) + \varepsilon N_{pqi}(\xi)\dfrac{\partial u_q^0(x)}{\partial x_p} + O(\varepsilon^2) & \text{if } x \in \Pi^\varepsilon, \end{cases}$$

where $\xi = x/\varepsilon$, $x \in \Omega$, $\xi \in Y \cap \varepsilon^{-1}(\Omega^\varepsilon \cup D^\varepsilon)$, and $\Pi^\varepsilon = \Omega^\varepsilon \cap \{x : |x_1| < Y\varepsilon/2\}$. Here, $(u_i^0)_n$ is the solution of the macroproblem with the new normal contact stiffness, and $(\Theta_p)_{n\times n}$ and $(N_{pqk})_{n\times n\times n}$ are periodic solutions of the following auxiliary problems on the periodicity cell:

$$\begin{aligned} \partial_j(a_{ijkl}\partial_l\Theta_k(\xi)) &= \frac{b|S_C|}{|Y|}, && \xi \in Y, \\ \left.\begin{aligned} \sigma_N(\xi) &:= a_{ijkl}\partial_l\Theta_k(\xi)n_j(\xi)n_i(\xi) = k_n \\ \sigma_{iT}(\xi) &:= a_{ijkl}\partial_l\Theta_k(\xi)n_j(\xi) - \sigma_N n_i(\xi) = \mu k_n \end{aligned}\right\} && \xi \in S_C, \\ \sigma_{ij}n_j(\xi) &:= a_{ijkl}\partial_l\Theta_k(\xi)n_j(\xi) = 0 && x \in S_N \\ \Theta_i \in H^1_{per}(Y), &\qquad \int_Y \Theta_i(\xi)d\xi = 0, && i = 1,2,3. \end{aligned} \tag{72}$$

$$\begin{aligned} \partial_j(a_{ijkl}\partial_l(N_{pqk}(\xi) + \xi_p\delta_{qk})) &= 0, && \xi \in Y, \\ a_{ijkl}\partial_l(N_{pqk}(\xi) + \xi_p\delta_{qk})n_j &= 0 && S_C \cup S_N, \\ N_{pqk} \in H^1_{per}(Y), &\qquad \int_Y N_{pqk}(\xi)d\xi = 0, && p,q,k = 1,2,3. \end{aligned} \tag{73}$$

The following approximation to the micro-stresses in the contact layer Π^ε is derived on the formal way:

$$\sigma_{ij}^\varepsilon(x,\xi) \approx a_{ijkl}\frac{\partial\Theta_{kp}(\xi)}{\partial\xi_l}u_p^0(x) + a_{ijkl}\frac{\partial}{\partial\xi_l}\Big(N_{pqk}(\xi) + \xi_p\delta_{qk}\Big)\frac{\partial u_q^0(x)}{\partial x_p} + O(\varepsilon). \tag{74}$$

Let us rewrite this approximation in a more visual form:

$$\sigma_{ij}^{ap}(x,\xi) = \sigma_{ij}\left(\Theta_p(\xi)\right)u_p^0(x) + (a_{lmpq})^{-1}\sigma_{lm}\left(N_{pq}(\xi) + \xi_p I\right)\sigma_{ij}\left(u^0(x)\right). \tag{75}$$

To predict the appearance of fracture, we need to use one or another *strength condition*:

$$\sup_{x\in\Omega^\varepsilon}\sigma_{\rm eq}(\sigma_{ij}^\varepsilon(x,\xi)) < \sigma_{\rm u}. \tag{76}$$

Here $\sigma_{\rm u}$ is the ultimate stress for the weakest of the contacting materials, and $\sigma_{\rm eq}$ is the equivalent stress, which can be chosen in accordance with one of the familiar strength conditions (von Mises or Tresca):

$$\sigma_{\rm eq}(\sigma_{ij}(x)) = \sqrt{\tfrac{3}{2}s_{kl}(x)s_{kl}(x)}, \qquad \sigma_{\rm eq}(\sigma_{ij}(x)) = \max_{k,l=1,\dots,3}|\sigma_k(x) - \sigma_l(x)|, \tag{77}$$

where $s_{ij} = \sigma_{ij} - \frac{1}{3}\delta_{ij}\sigma_{kk}$. It is proved in [13] that as soon as $\sigma_{ij}^\varepsilon(x)$ two-scale converge to $\sigma_{ij}^{ap}(x,\xi)$, the *macrostrength condition for the contact layer* becomes

$$\sup_{\hat{x}\in S_0}\sup_{\xi\in Y}\sigma_{\rm eq}(\sigma_{ij}^{ap}(x,\xi)) < \sigma_{\rm u}, \tag{78}$$

From the practical point of view this means that as soon as solutions of the homogenized problem and the problems for Θ_p and N_{pqk} are found, the macrostrength in the boundary layer can be estimated by the last relation.

4.2 Application Example

As an example for the contact problem, we consider a contact between cementless hip-prosthesis with the bone. The surface of the implant is coated by a thin layer with microvalleys and pores. The microgeometry and elastic properties of the coating as well as the macrogeometry of the bone and prosthesis and their elastic properties are known. We denote by a small parameter, ε, the ratio of the characteristic dimension of the interface irregularities to the characteristic length of the bone-implant interaction zone.
A detailed numerical analysis of the problem is given in [15] In this paper we simplify the numerical illustration through the consideration of the micro-contact roughness of the same size and with a plane base.

4.3 Numerical Solution

In computations, the finite element software package ANSYS was used. The materials of the implant and bone were assumed homogeneous and isotropic with Young's moduli $E_{\rm impl} = 100\,$GPa and $E_{\rm bone} = 9\,$GPa, Poisson's ratios $\nu_{\rm impl} = 0.30\,$GPa and $\nu_{\rm bone} = 0.27\,$GPa, Coulomb's friction with the coefficient $\mu = 0.3$, and normal contact stiffness $k_n^\varepsilon = 200\,$GPa.

First we considered the microcontact problem for Θ for a unit cell. The geometry of contact regions is depicted in Fig. 6 and the contact, boundary, and symmetry conditions are shown in Fig. 7. The implant coating hills were taken to be rectangular parallelepipeds square in plan with side $a = 0.4$ (here a is dimensionless but typically it ranges between 5 and $500\,\mu$m). Due to symmetry, only one eighth of the unit cell was studied. The corresponding distribution of von Mises stresses is presented in Fig. 8.

Further we considered a macrocontact problem for the axisymmetric bone-implant system shown in Fig. 9. The femur bone is modeled by a hollow cylinder fully clamped at the base. The implant is modeled by a solid cylinder whose lower part has the shape of a frustum of a cone. The radius of the upper part of the cylinder slightly exceeds the interior radius of the bone, which means that the implant tightly fits into the bone and the structure is in a prestrained state. The dimensions are shown in Fig. 9. A pressure of $1\,$MPa is applied to the top end of the implant, which approximately corresponds to half the weight of a patient. We have $k_n^0 = (a^2/Y_0^2)k_n^\varepsilon = 32\,$GPa for the homogenized normal contact stiffness.

Figures 10(a)–(d) depict the computation results for the macrocontact problem under consideration. The axial stress field has regions of increased stresses near the points where the implant detaches from the bone. These are corner points, where the stem geometry changes from cylindrical to conical, and points of change of boundary conditions. Mathematically, stress singularities can occur at such points. As one should expect, the maximal equivalent stresses arise near the contact interface.

5 Conclusions for Mechanical Foundations

We want to recall all main factors that influence the macro-contact conditions, based on the estimations of Sections 2.8, 3.2.2. Since the macro-contact stiffness and tangential drag forces are proportional to the micro-contact stiffness, which is further proportional to the Young's and share moduli of the contacting materials, some changes in the micro-stiffness of the contacting materials will cause the respective change in the macro-stiffness. The next parameter causing the influence is the measure (total length or area) of the contact micro-surface. The grater is is the contact surface measure, the higher is the contact macro-stiffness. The last influencing factor is the greatest slope of the local normal to each cavity surface with respect to the global normal to the macro-contact surface

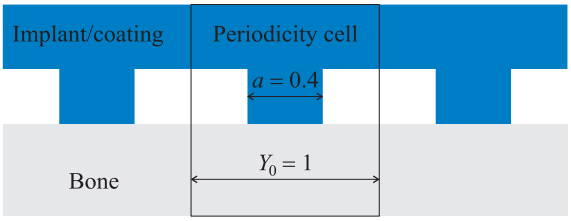

Figure 6: Microgeometry of contact domains

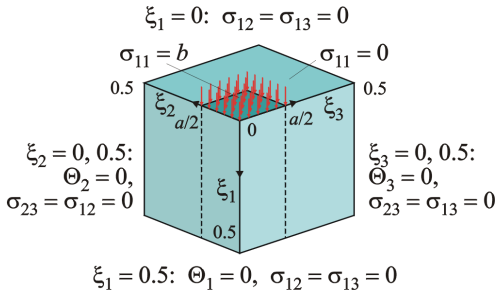

Figure 7: One eighth of the periodicity cell. Boundary conditions for the Θ-problem

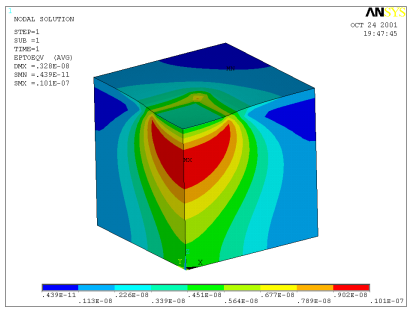

Figure 8: Von Mises equivalent stress in the periodicity cell, $\tilde{\sigma}_{\mathrm{eq}}(\Theta(\xi))$

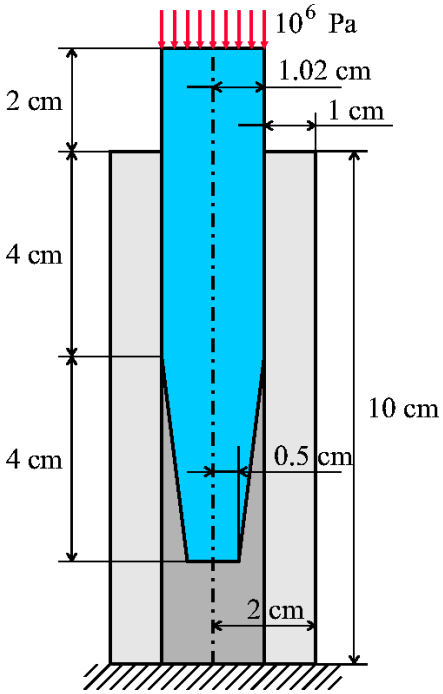

Figure 9: Macrocontact of a bone with a hip prosthesis

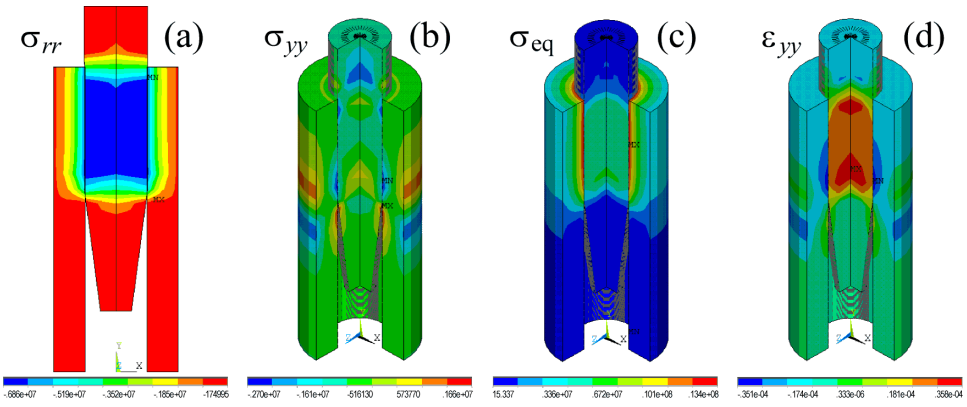

Figure 10: Stress and strain distributions in the macrocontact problem: (a) radial stresses (frontal view), (b) axial stresses (isometric view), (c) equivalent von Mises stresses, and (d) equivalent von Mises strains

at the place of this cavity, i.e. the sharpness of the micro-surface cavities. The contact macrostiffness can be increased by the increasing of the microroughness's sharpness.
We recall again the fact that starting with the frictionless contact micro-problem with a rough interface, we end up with the macro-problem containing some tangential drag forces on the contact surface.

6 Acknowledgment

The research presented in this paper was carried out under the financial support from the grant to European CRAFT-Project IST-1999-56408 and applied by mechanical engineers from the world-leading orthopedic institute Rizzoli, Bologna as well as by some small French and Italian hip-prosthesis' producing companies.

References

[1] Allaire, G., Homogenization and Two-Scale Convergence, SIAM J. Math. Anal., 1992, Vol. 23, 1482–1518.

[2] G.Allaire, A.Damlamian and U.Hornung, Two-Scale Convergence on Periodic Surfaces and Applications, Proceedings of the "Congres International sur la Modlisation Mathmatique des Ecoulements en Milieux Poreux, Saint Etienne, 22 au 26 mai 1995", 1995.

[3] Belyaev, A. G., Piatnitski, A. L., and Chechkin, G. A., Asymptotic behaviour of a solution to a boundary value problem in a perforated domain with oscillating boundary, Sib. Math. J., Vol. 39, No. 4, 621–44, 1998

[4] Chechkin, G. A., Friedman, A., Piatnitski, A. L., The boundary-value problem in domains with very rapidly oscillating boundary, J. Math. An. and Appl., 231, 213–234, 1999

[5] Duvaut, G., Lions, J. L., Inequalities in Mechanics and Physics, Springer-Verlag, 1976

[6] Eck, C., Jarusek, J., Existence results for the static contact problem with Coulomb friction, Mathematical Models and Methods in Applied Sciences, 1998, Vol. 8, No. 3, 445-468

[7] Han, W., On the Numerical Approximation of a Frictional Contact Problem with Normal Compliance, Numer. Funct. Anal. and Optimiz., 1996, 17(3& 4), 307-321

[8] Hansson, S. and Norton, M., The relation between surface roughness and interfacial shear strength for bone-anchored implants. A mathematical model, J. Biomech., 1999, Vol. 32, 829–36

[9] Hornung, U., Homogenization and Porous Media, Springer, 1997

[10] Jäger, W., Oleinik, O. A., and Shaposhnikova, T. A., Homogenization of solutions of the Poisson equation in a domain perforated along a hypersurface, with mixed boundary conditions on the boundary of the cavities, Trans. Moscow Math. Soc., 1998, Vol. 59, 135–57

[11] Jäger, W., Oleinik, O. A., and Shaposhnikova, T. A., On homogenization of solutions of the Poisson equation in a perforated domain with different types of boundary conditions on different cavities, Applicable Analysis, 1997, Vol. 65, 205–23

[12] Kikuchi, N., Oden J.T., Contact Problems in Elasticity: A Stady of Variational Inequalities and Finite Element Methods, SIAM Philadelphia, 1988

[13] Mikhailov, S. E., Orlik, J., Asymptotic homogenization in strength and fatigue durability analysis of composites, Proceedings of IUTAM Symposium 02/4 "Singularities, Asymptotics and Homogenisation in Problems of Mechanics"(July 8-11, 2002) Univ. of Liverpool, UK, Kluwer 2002.

[14] Orlik, J., Transmission and homogenization in hereditary viscoelasticity with ageing and shrinkage, PhD-Thesis, Shaker Verlag, 2000

[15] Orlik, J., Zhurov, A., and Middleton, J., On the secondary stability of coated cementless hip replacement: parameters that affect interface strength, Med Engng & Phys, Vol. 25, Issue 10, p. 825-831, Dec. 2003

[16] Yosifian, G. A., Some Unilateral Boundary Value Problems for Elastic Bodies with Rugged Boundaries, J. Math. Sci., New York 108, No.4, 574-607 (2002); translation from Tr. Semin. Im. I. G. Petrovskogo 21, 240-297, 2001

[17] Yosifian, G.A., On some homogenization problems in perforated domains with nonlinear boundary conditions. (English) Appl. Anal. 65, No.3-4, 257-288, 1997

Published reports of the Fraunhofer ITWM

The PDF-files of the following reports are available under:
www.itwm.fraunhofer.de/rd/presse/berichte

1. D. Hietel, K. Steiner, J. Struckmeier

A Finite - Volume Particle Method for Compressible Flows

We derive a new class of particle methods for conservation laws, which are based on numerical flux functions to model the interactions between moving particles. The derivation is similar to that of classical Finite-Volume methods; except that the fixed grid structure in the Finite-Volume method is substituted by so-called mass packets of particles. We give some numerical results on a shock wave solution for Burgers equation as well as the well-known one-dimensional shock tube problem.
(19 pages, 1998)

2. M. Feldmann, S. Seibold

Damage Diagnosis of Rotors: Application of Hilbert Transform and Multi-Hypothesis Testing

In this paper, a combined approach to damage diagnosis of rotors is proposed. The intention is to employ signal-based as well as model-based procedures for an improved detection of size and location of the damage. In a first step, Hilbert transform signal processing techniques allow for a computation of the signal envelope and the instantaneous frequency, so that various types of non-linearities due to a damage may be identified and classified based on measured response data. In a second step, a multi-hypothesis bank of Kalman Filters is employed for the detection of the size and location of the damage based on the information of the type of damage provided by the results of the Hilbert transform.
Keywords: Hilbert transform, damage diagnosis, Kalman filtering, non-linear dynamics
(23 pages, 1998)

3. Y. Ben-Haim, S. Seibold

Robust Reliability of Diagnostic Multi-Hypothesis Algorithms: Application to Rotating Machinery

Damage diagnosis based on a bank of Kalman filters, each one conditioned on a specific hypothesized system condition, is a well recognized and powerful diagnostic tool. This multi-hypothesis approach can be applied to a wide range of damage conditions. In this paper, we will focus on the diagnosis of cracks in rotating machinery. The question we address is: how to optimize the multi-hypothesis algorithm with respect to the uncertainty of the spatial form and location of cracks and their resulting dynamic effects. First, we formulate a measure of the reliability of the diagnostic algorithm, and then we discuss modifications of the diagnostic algorithm for the maximization of the reliability. The reliability of a diagnostic algorithm is measured by the amount of uncertainty consistent with no-failure of the diagnosis. Uncertainty is quantitatively represented with convex models.
Keywords: Robust reliability, convex models, Kalman filtering, multi-hypothesis diagnosis, rotating machinery, crack diagnosis
(24 pages, 1998)

4. F.-Th. Lentes, N. Siedow

Three-dimensional Radiative Heat Transfer in Glass Cooling Processes

For the numerical simulation of 3D radiative heat transfer in glasses and glass melts, practically applicable mathematical methods are needed to handle such problems optimal using workstation class computers. Since the exact solution would require super-computer capabilities we concentrate on approximate solutions with a high degree of accuracy. The following approaches are studied: 3D diffusion approximations and 3D ray-tracing methods.
(23 pages, 1998)

5. A. Klar, R. Wegener

A hierarchy of models for multilane vehicular traffic
Part I: Modeling

In the present paper multilane models for vehicular traffic are considered. A microscopic multilane model based on reaction thresholds is developed. Based on this model an Enskog like kinetic model is developed. In particular, care is taken to incorporate the correlations between the vehicles. From the kinetic model a fluid dynamic model is derived. The macroscopic coefficients are deduced from the underlying kinetic model. Numerical simulations are presented for all three levels of description in [10]. Moreover, a comparison of the results is given there.
(23 pages, 1998)

Part II: Numerical and stochastic investigations

In this paper the work presented in [6] is continued. The present paper contains detailed numerical investigations of the models developed there. A numerical method to treat the kinetic equations obtained in [6] are presented and results of the simulations are shown. Moreover, the stochastic correlation model used in [6] is described and investigated in more detail.
(17 pages, 1998)

6. A. Klar, N. Siedow

Boundary Layers and Domain Decomposition for Radiative Heat Transfer and Diffusion Equations: Applications to Glass Manufacturing Processes

In this paper domain decomposition methods for radiative transfer problems including conductive heat transfer are treated. The paper focuses on semi-transparent materials, like glass, and the associated conditions at the interface between the materials. Using asymptotic analysis we derive conditions for the coupling of the radiative transfer equations and a diffusion approximation. Several test cases are treated and a problem appearing in glass manufacturing processes is computed. The results clearly show the advantages of a domain decomposition approach. Accuracy equivalent to the solution of the global radiative transfer solution is achieved, whereas computation time is strongly reduced.
(24 pages, 1998)

7. I. Choquet

Heterogeneous catalysis modelling and numerical simulation in rarified gas flows Part I: Coverage locally at equilibrium

A new approach is proposed to model and simulate numerically heterogeneous catalysis in rarefied gas flows. It is developed to satisfy all together the following points:
1) describe the gas phase at the microscopic scale, as required in rarefied flows,
2) describe the wall at the macroscopic scale, to avoid prohibitive computational costs and consider not only crystalline but also amorphous surfaces,
3) reproduce on average macroscopic laws correlated with experimental results and
4) derive analytic models in a systematic and exact way. The problem is stated in the general framework of a non static flow in the vicinity of a catalytic and non porous surface (without aging). It is shown that the exact and systematic resolution method based on the Laplace transform, introduced previously by the author to model collisions in the gas phase, can be extended to the present problem. The proposed approach is applied to the modelling of the EleyRideal and LangmuirHinshelwood recombinations, assuming that the coverage is locally at equilibrium. The models are developed considering one atomic species and extended to the general case of several atomic species. Numerical calculations show that the models derived in this way reproduce with accuracy behaviors observed experimentally.
(24 pages, 1998)

8. J. Ohser, B. Steinbach, C. Lang

Efficient Texture Analysis of Binary Images

A new method of determining some characteristics of binary images is proposed based on a special linear filtering. This technique enables the estimation of the area fraction, the specific line length, and the specific integral of curvature. Furthermore, the specific length of the total projection is obtained, which gives detailed information about the texture of the image. The influence of lateral and directional resolution depending on the size of the applied filter mask is discussed in detail. The technique includes a method of increasing directional resolution for texture analysis while keeping lateral resolution as high as possible.
(17 pages, 1998)

9. J. Orlik

Homogenization for viscoelasticity of the integral type with aging and shrinkage

A multiphase composite with periodic distributed inclusions with a smooth boundary is considered in this contribution. The composite component materials are supposed to be linear viscoelastic and aging (of the nonconvolution integral type, for which the Laplace transform with respect to time is not effectively applicable) and are subjected to isotropic shrinkage. The free shrinkage deformation can be considered as a fictitious temperature deformation in the behavior law. The procedure presented in this paper proposes a way to determine average (effective homogenized) viscoelastic and shrinkage (temperature) composite properties and the homogenized stressfield from known properties of the components. This is done by the extension of the asymptotic homogenization technique known for pure elastic nonhomogeneous bodies to the nonhomogeneous thermoviscoelasticity of the integral noncon-

volution type. Up to now, the homogenization theory has not covered viscoelasticity of the integral type. SanchezPalencia (1980), Francfort & Suquet (1987) (see [2], [9]) have considered homogenization for viscoelasticity of the differential form and only up to the first derivative order. The integralmodeled viscoelasticity is more general then the differential one and includes almost all known differential models. The homogenization procedure is based on the construction of an asymptotic solution with respect to a period of the composite structure. This reduces the original problem to some auxiliary boundary value problems of elasticity and viscoelasticity on the unit periodic cell, of the same type as the original non-homogeneous problem. The existence and uniqueness results for such problems were obtained for kernels satisfying some constrain conditions. This is done by the extension of the Volterra integral operator theory to the Volterra operators with respect to the time, whose 1 kernels are space linear operators for any fixed time variables. Some ideas of such approach were proposed in [11] and [12], where the Volterra operators with kernels depending additionally on parameter were considered. This manuscript delivers results of the same nature for the case of the spaceoperator kernels.
(20 pages, 1998)

10. J. Mohring

Helmholtz Resonators with Large Aperture

The lowest resonant frequency of a cavity resonator is usually approximated by the classical Helmholtz formula. However, if the opening is rather large and the front wall is narrow this formula is no longer valid. Here we present a correction which is of third order in the ratio of the diameters of aperture and cavity. In addition to the high accuracy it allows to estimate the damping due to radiation. The result is found by applying the method of matched asymptotic expansions. The correction contains form factors describing the shapes of opening and cavity. They are computed for a number of standard geometries. Results are compared with numerical computations.
(21 pages, 1998)

11. H. W. Hamacher, A. Schöbel

On Center Cycles in Grid Graphs

Finding "good" cycles in graphs is a problem of great interest in graph theory as well as in locational analysis. We show that the center and median problems are NP hard in general graphs. This result holds both for the variable cardinality case (i.e. all cycles of the graph are considered) and the fixed cardinality case (i.e. only cycles with a given cardinality p are feasible). Hence it is of interest to investigate special cases where the problem is solvable in polynomial time. In grid graphs, the variable cardinality case is, for instance, trivially solvable if the shape of the cycle can be chosen freely. If the shape is fixed to be a rectangle one can analyze rectangles in grid graphs with, in sequence, fixed dimension, fixed cardinality, and variable cardinality. In all cases a complete characterization of the optimal cycles and closed form expressions of the optimal objective values are given, yielding polynomial time algorithms for all cases of center rectangle problems. Finally, it is shown that center cycles can be chosen as rectangles for small cardinalities such that the center cycle problem in grid graphs is in these cases completely solved.
(15 pages, 1998)

12. H. W. Hamacher, K.-H. Küfer

Inverse radiation therapy planning - a multiple objective optimisation approach

For some decades radiation therapy has been proved successful in cancer treatment. It is the major task of clinical radiation treatment planning to realize on the one hand a high level dose of radiation in the cancer tissue in order to obtain maximum tumor control. On the other hand it is obvious that it is absolutely necessary to keep in the tissue outside the tumor, particularly in organs at risk, the unavoidable radiation as low as possible.
No doubt, these two objectives of treatment planning - high level dose in the tumor, low radiation outside the tumor - have a basically contradictory nature. Therefore, it is no surprise that inverse mathematical models with dose distribution bounds tend to be infeasible in most cases. Thus, there is need for approximations compromising between overdosing the organs at risk and underdosing the target volume.
Differing from the currently used time consuming iterative approach, which measures deviation from an ideal (non-achievable) treatment plan using recursively trial-and-error weights for the organs of interest, we go a new way trying to avoid a priori weight choices and consider the treatment planning problem as a multiple objective linear programming problem: with each organ of interest, target tissue as well as organs at risk, we associate an objective function measuring the maximal deviation from the prescribed doses.
We build up a data base of relatively few efficient solutions representing and approximating the variety of Pareto solutions of the multiple objective linear programming problem. This data base can be easily scanned by physicians looking for an adequate treatment plan with the aid of an appropriate online tool.
(14 pages, 1999)

13. C. Lang, J. Ohser, R. Hilfer

On the Analysis of Spatial Binary Images

This paper deals with the characterization of microscopically heterogeneous, but macroscopically homogeneous spatial structures. A new method is presented which is strictly based on integral-geometric formulae such as Crofton's intersection formulae and Hadwiger's recursive definition of the Euler number. The corresponding algorithms have clear advantages over other techniques. As an example of application we consider the analysis of spatial digital images produced by means of Computer Assisted Tomography.
(20 pages, 1999)

14. M. Junk

On the Construction of Discrete Equilibrium Distributions for Kinetic Schemes

A general approach to the construction of discrete equilibrium distributions is presented. Such distribution functions can be used to set up Kinetic Schemes as well as Lattice Boltzmann methods. The general principles are also applied to the construction of Chapman Enskog distributions which are used in Kinetic Schemes for compressible Navier-Stokes equations.
(24 pages, 1999)

15. M. Junk, S. V. Raghurame Rao

A new discrete velocity method for Navier-Stokes equations

The relation between the Lattice Boltzmann Method, which has recently become popular, and the Kinetic Schemes, which are routinely used in Computational Fluid Dynamics, is explored. A new discrete velocity model for the numerical solution of Navier-Stokes equations for incompressible fluid flow is presented by combining both the approaches. The new scheme can be interpreted as a pseudo-compressibility method and, for a particular choice of parameters, this interpretation carries over to the Lattice Boltzmann Method.
(20 pages, 1999)

16. H. Neunzert

Mathematics as a Key to Key Technologies

The main part of this paper will consist of examples, how mathematics really helps to solve industrial problems; these examples are taken from our Institute for Industrial Mathematics, from research in the Technomathematics group at my university, but also from ECMI groups and a company called TecMath, which originated 10 years ago from my university group and has already a very successful history.
(39 pages (4 PDF-Files), 1999)

17. J. Ohser, K. Sandau

Considerations about the Estimation of the Size Distribution in Wicksell's Corpuscle Problem

Wicksell's corpuscle problem deals with the estimation of the size distribution of a population of particles, all having the same shape, using a lower dimensional sampling probe. This problem was originary formulated for particle systems occurring in life sciences but its solution is of actual and increasing interest in materials science. From a mathematical point of view, Wicksell's problem is an inverse problem where the interesting size distribution is the unknown part of a Volterra equation. The problem is often regarded ill-posed, because the structure of the integrand implies unstable numerical solutions. The accuracy of the numerical solutions is considered here using the condition number, which allows to compare different numerical methods with different (equidistant) class sizes and which indicates, as one result, that a finite section thickness of the probe reduces the numerical problems. Furthermore, the relative error of estimation is computed which can be split into two parts. One part consists of the relative discretization error that increases for increasing class size, and the second part is related to the relative statistical error which increases with decreasing class size. For both parts, upper bounds can be given and the sum of them indicates an optimal class width depending on some specific constants.
(18 pages, 1999)

18. E. Carrizosa, H. W. Hamacher, R. Klein, S. Nickel

Solving nonconvex planar location problems by finite dominating sets

It is well-known that some of the classical location problems with polyhedral gauges can be solved in polynomial time by finding a finite dominating set, i.e. a finite set of candidates guaranteed to contain at least one optimal location.
In this paper it is first established that this result holds

for a much larger class of problems than currently considered in the literature. The model for which this result can be proven includes, for instance, location problems with attraction and repulsion, and location-allocation problems.
Next, it is shown that the approximation of general gauges by polyhedral ones in the objective function of our general model can be analyzed with regard to the subsequent error in the optimal objective value. For the approximation problem two different approaches are described, the sandwich procedure and the greedy algorithm. Both of these approaches lead - for fixed epsilon - to polynomial approximation algorithms with accuracy epsilon for solving the general model considered in this paper.
Keywords: Continuous Location, Polyhedral Gauges, Finite Dominating Sets, Approximation, Sandwich Algorithm, Greedy Algorithm
(19 pages, 2000)

19. A. Becker

A Review on Image Distortion Measures

Within this paper we review image distortion measures. A distortion measure is a criterion that assigns a "quality number" to an image. We distinguish between mathematical distortion measures and those distortion measures in-cooperating a priori knowledge about the imaging devices (e. g. satellite images), image processing algorithms or the human physiology. We will consider representative examples of different kinds of distortion measures and are going to discuss them.
Keywords: Distortion measure, human visual system
(26 pages, 2000)

20. H. W. Hamacher, M. Labbé, S. Nickel, T. Sonneborn

Polyhedral Properties of the Uncapacitated Multiple Allocation Hub Location Problem

We examine the feasibility polyhedron of the uncapacitated hub location problem (UHL) with multiple allocation, which has applications in the fields of air passenger and cargo transportation, telecommunication and postal delivery services. In particular we determine the dimension and derive some classes of facets of this polyhedron. We develop some general rules about lifting facets from the uncapacitated facility location (UFL) for UHL and projecting facets from UHL to UFL. By applying these rules we get a new class of facets for UHL which dominates the inequalities in the original formulation. Thus we get a new formulation of UHL whose constraints are all facet–defining. We show its superior computational performance by benchmarking it on a well known data set.
Keywords: integer programming, hub location, facility location, valid inequalities, facets, branch and cut
(21 pages, 2000)

21. H. W. Hamacher, A. Schöbel

Design of Zone Tariff Systems in Public Transportation

Given a public transportation system represented by its stops and direct connections between stops, we consider two problems dealing with the prices for the customers: The fare problem in which subsets of stops are already aggregated to zones and "good" tariffs have to be found in the existing zone system. Closed form solutions for the fare problem are presented for three objective functions. In the zone problem the design of the zones is part of the problem. This problem is NP hard and we therefore propose three heuristics which prove to be very successful in the redesign of one of Germany's transportation systems.
(30 pages, 2001)

22. D. Hietel, M. Junk, R. Keck, D. Teleaga:

The Finite-Volume-Particle Method for Conservation Laws

In the Finite-Volume-Particle Method (FVPM), the weak formulation of a hyperbolic conservation law is discretized by restricting it to a discrete set of test functions. In contrast to the usual Finite-Volume approach, the test functions are not taken as characteristic functions of the control volumes in a spatial grid, but are chosen from a partition of unity with smooth and overlapping partition functions (the particles), which can even move along pre- scribed velocity fields. The information exchange between particles is based on standard numerical flux functions. Geometrical information, similar to the surface area of the cell faces in the Finite-Volume Method and the corresponding normal directions are given as integral quantities of the partition functions. After a brief derivation of the Finite-Volume-Particle Method, this work focuses on the role of the geometric coefficients in the scheme.
(16 pages, 2001)

23. T. Bender, H. Hennes, J. Kalcsics, M. T. Melo, S. Nickel

Location Software and Interface with GIS and Supply Chain Management

The objective of this paper is to bridge the gap between location theory and practice. To meet this objective focus is given to the development of software capable of addressing the different needs of a wide group of users. There is a very active community on location theory encompassing many research fields such as operations research, computer science, mathematics, engineering, geography, economics and marketing. As a result, people working on facility location problems have a very diverse background and also different needs regarding the software to solve these problems. For those interested in non-commercial applications (e. g. students and researchers), the library of location algorithms (LoLA can be of considerable assistance. LoLA contains a collection of efficient algorithms for solving planar, network and discrete facility location problems. In this paper, a detailed description of the functionality of LoLA is presented. In the fields of geography and marketing, for instance, solving facility location problems requires using large amounts of demographic data. Hence, members of these groups (e. g. urban planners and sales managers) often work with geographical information too s. To address the specific needs of these users, LoLA was inked to a geographical information system (GIS) and the details of the combined functionality are described in the paper. Finally, there is a wide group of practitioners who need to solve large problems and require special purpose software with a good data interface. Many of such users can be found, for example, in the area of supply chain management (SCM). Logistics activities involved in strategic SCM include, among others, facility location planning. In this paper, the development of a commercial location software tool is also described. The too is embedded in the Advanced Planner and Optimizer SCM software developed by SAP AG, Walldorf, Germany. The paper ends with some conclusions and an outlook to future activities.
Keywords: facility location, software development, geographical information systems, supply chain management.
(48 pages, 2001)

24. H. W. Hamacher, S. A. Tjandra

Mathematical Modelling of Evacuation Problems: A State of Art

This paper details models and algorithms which can be applied to evacuation problems. While it concentrates on building evacuation many of the results are applicable also to regional evacuation. All models consider the time as main parameter, where the travel time between components of the building is part of the input and the overall evacuation time is the output. The paper distinguishes between macroscopic and microscopic evacuation models both of which are able to capture the evacuees' movement over time.
Macroscopic models are mainly used to produce good lower bounds for the evacuation time and do not consider any individual behavior during the emergency situation. These bounds can be used to analyze existing buildings or help in the design phase of planning a building. Macroscopic approaches which are based on dynamic network flow models (minimum cost dynamic flow, maximum dynamic flow, universal maximum flow, quickest path and quickest flow) are described. A special feature of the presented approach is the fact, that travel times of evacuees are not restricted to be constant, but may be density dependent. Using multicriteria optimization priority regions and blockage due to fire or smoke may be considered. It is shown how the modelling can be done using time parameter either as discrete or continuous parameter.
Microscopic models are able to model the individual evacuee's characteristics and the interaction among evacuees which influence their movement. Due to the corresponding huge amount of data one uses simulation approaches. Some probabilistic laws for individual evacuee's movement are presented. Moreover ideas to model the evacuee's movement using cellular automata (CA) and resulting software are presented. In this paper we will focus on macroscopic models and only summarize some of the results of the microscopic approach. While most of the results are applicable to general evacuation situations, we concentrate on building evacuation.
(44 pages, 2001)

25. J. Kuhnert, S. Tiwari

Grid free method for solving the Poisson equation

A Grid free method for solving the Poisson equation is presented. This is an iterative method. The method is based on the weighted least squares approximation in which the Poisson equation is enforced to be satisfied in every iterations. The boundary conditions can also be enforced in the iteration process. This is a local approximation procedure. The Dirichlet, Neumann and mixed boundary value problems on a unit square are presented and the analytical solutions are compared with the exact solutions. Both solutions matched perfectly.
Keywords: Poisson equation, Least squares method, Grid free method
(19 pages, 2001)

26. T. Götz, H. Rave, D. Reinel-Bitzer, K. Steiner, H. Tiemeier

Simulation of the fiber spinning process

To simulate the influence of process parameters to the melt spinning process a fiber model is used and coupled with CFD calculations of the quench air flow. In the fiber model energy, momentum and mass balance are solved for the polymer mass flow. To calculate the quench air the Lattice Boltzmann method is used. Simulations and experiments for different process parameters and hole configurations are compared and show a good agreement.

Keywords: Melt spinning, fiber model, Lattice Boltzmann, CFD

(19 pages, 2001)

27. A. Zemitis

On interaction of a liquid film with an obstacle

In this paper mathematical models for liquid films generated by impinging jets are discussed. Attention is stressed to the interaction of the liquid film with some obstacle. S. G. Taylor [Proc. R. Soc. London Ser. A 253, 313 (1959)] found that the liquid film generated by impinging jets is very sensitive to properties of the wire which was used as an obstacle. The aim of this presentation is to propose a modification of the Taylor's model, which allows to simulate the film shape in cases, when the angle between jets is different from 180°. Numerical results obtained by discussed models give two different shapes of the liquid film similar as in Taylors experiments. These two shapes depend on the regime: either droplets are produced close to the obstacle or not. The difference between two regimes becomes larger if the angle between jets decreases. Existence of such two regimes can be very essential for some applications of impinging jets, if the generated liquid film can have a contact with obstacles.

Keywords: impinging jets, liquid film, models, numerical solution, shape

(22 pages, 2001)

28. I. Ginzburg, K. Steiner

Free surface lattice-Boltzmann method to model the filling of expanding cavities by Bingham Fluids

The filling process of viscoplastic metal alloys and plastics in expanding cavities is modelled using the lattice Boltzmann method in two and three dimensions. These models combine the regularized Bingham model for viscoplastic with a free-interface algorithm. The latter is based on a modified immiscible lattice Boltzmann model in which one species is the fluid and the other one is considered as vacuum. The boundary conditions at the curved liquid-vacuum interface are met without any geometrical front reconstruction from a first-order Chapman-Enskog expansion. The numerical results obtained with these models are found in good agreement with available theoretical and numerical analysis.

Keywords: Generalized LBE, free-surface phenomena, interface boundary conditions, filling processes, Bingham viscoplastic model, regularized models

(22 pages, 2001)

29. H. Neunzert

»Denn nichts ist für den Menschen als Menschen etwas wert, was er nicht mit Leidenschaft tun kann«

Vortrag anlässlich der Verleihung des Akademiepreises des Landes Rheinland-Pfalz am 21.11.2001

Was macht einen guten Hochschullehrer aus? Auf diese Frage gibt es sicher viele verschiedene, fachbezogene Antworten, aber auch ein paar allgemeine Gesichtspunkte: es bedarf der »Leidenschaft« für die Forschung (Max Weber), aus der dann auch die Begeisterung für die Lehre erwächst. Forschung und Lehre gehören zusammen, um die Wissenschaft als lebendiges Tun vermitteln zu können. Der Vortrag gibt Beispiele dafür, wie in angewandter Mathematik Forschungsaufgaben aus praktischen Alltagsproblemstellungen erwachsen, die in die Lehre auf verschiedenen Stufen (Gymnasium bis Graduiertenkolleg) einfließen; er leitet damit auch zu einem aktuellen Forschungsgebiet, der Mehrskalenanalyse mit ihren vielfältigen Anwendungen in Bildverarbeitung, Materialentwicklung und Strömungsmechanik über, was aber nur kurz gestreift wird. Mathematik erscheint hier als eine moderne Schlüsseltechnologie, die aber auch enge Beziehungen zu den Geistes- und Sozialwissenschaften hat.

Keywords: Lehre, Forschung, angewandte Mathematik, Mehrskalenanalyse, Strömungsmechanik

(18 pages, 2001)

30. J. Kuhnert, S. Tiwari

Finite pointset method based on the projection method for simulations of the incompressible Navier-Stokes equations

A Lagrangian particle scheme is applied to the projection method for the incompressible Navier-Stokes equations. The approximation of spatial derivatives is obtained by the weighted least squares method. The pressure Poisson equation is solved by a local iterative procedure with the help of the least squares method. Numerical tests are performed for two dimensional cases. The Couette flow, Poiseuelle flow, decaying shear flow and the driven cavity flow are presented. The numerical solutions are obtained for stationary as well as instationary cases and are compared with the analytical solutions for channel flows. Finally, the driven cavity in a unit square is considered and the stationary solution obtained from this scheme is compared with that from the finite element method.

Keywords: Incompressible Navier-Stokes equations, Meshfree method, Projection method, Particle scheme, Least squares approximation

AMS subject classification: 76D05, 76M28

(25 pages, 2001)

31. R. Korn, M. Krekel

Optimal Portfolios with Fixed Consumption or Income Streams

We consider some portfolio optimisation problems where either the investor has a desire for an a priori specified consumption stream or/and follows a deterministic pay in scheme while also trying to maximize expected utility from final wealth. We derive explicit closed form solutions for continuous and discrete monetary streams. The mathematical method used is classical stochastic control theory.

Keywords: Portfolio optimisation, stochastic control, HJB equation, discretisation of control problems.

(23 pages, 2002)

32. M. Krekel

Optimal portfolios with a loan dependent credit spread

If an investor borrows money he generally has to pay higher interest rates than he would have received, if he had put his funds on a savings account. The classical model of continuous time portfolio optimisation ignores this effect. Since there is obviously a connection between the default probability and the total percentage of wealth, which the investor is in debt, we study portfolio optimisation with a control dependent interest rate. Assuming a logarithmic and a power utility function, respectively, we prove explicit formulae of the optimal control.

Keywords: Portfolio optimisation, stochastic control, HJB equation, credit spread, log utility, power utility, non-linear wealth dynamics

(25 pages, 2002)

33. J. Ohser, W. Nagel, K. Schladitz

The Euler number of discretized sets - on the choice of adjacency in homogeneous lattices

Two approaches for determining the Euler-Poincaré characteristic of a set observed on lattice points are considered in the context of image analysis { the integral geometric and the polyhedral approach. Information about the set is assumed to be available on lattice points only. In order to retain properties of the Euler number and to provide a good approximation of the true Euler number of the original set in the Euclidean space, the appropriate choice of adjacency in the lattice for the set and its background is crucial. Adjacencies are defined using tessellations of the whole space into polyhedrons. In R 3 , two new 14 adjacencies are introduced additionally to the well known 6 and 26 adjacencies. For the Euler number of a set and its complement, a consistency relation holds. Each of the pairs of adjacencies (14:1; 14:1), (14:2; 14:2), (6; 26), and (26; 6) is shown to be a pair of complementary adjacencies with respect to this relation. That is, the approximations of the Euler numbers are consistent if the set and its background (complement) are equipped with this pair of adjacencies. Furthermore, sufficient conditions for the correctness of the approximations of the Euler number are given. The analysis of selected microstructures and a simulation study illustrate how the estimated Euler number depends on the chosen adjacency. It also shows that there is not a uniquely best pair of adjacencies with respect to the estimation of the Euler number of a set in Euclidean space.

Keywords: image analysis, Euler number, neighborhod relationships, cuboidal lattice

(32 pages, 2002)

34. I. Ginzburg, K. Steiner

Lattice Boltzmann Model for Free-Surface flow and Its Application to Filling Process in Casting

A generalized lattice Boltzmann model to simulate free-surface is constructed in both two and three dimensions. The proposed model satisfies the interfacial boundary conditions accurately. A distinctive feature of the model is that the collision processes is carried out only on the points occupied partially or fully by the fluid. To maintain a sharp interfacial front, the method includes an anti-diffusion algorithm. The unknown distribution functions at the interfacial region are constructed according to the first order Chapman-Enskog analysis. The interfacial boundary conditions are satis-

fied exactly by the coefficients in the Chapman-Enskog expansion. The distribution functions are naturally expressed in the local interfacial coordinates. The macroscopic quantities at the interface are extracted from the least-square solutions of a locally linearized system obtained from the known distribution functions. The proposed method does not require any geometric front construction and is robust for any interfacial topology. Simulation results of realistic filling process are presented: rectangular cavity in two dimensions and Hammer box, Campbell box, Sheffield box, and Motorblock in three dimensions. To enhance the stability at high Reynolds numbers, various upwind-type schemes are developed. Free-slip and no-slip boundary conditions are also discussed.
Keywords: Lattice Boltzmann models; free-surface phenomena; interface boundary conditions; filling processes; injection molding; volume of fluid method; interface boundary conditions; advection-schemes; upwind-schemes
(54 pages, 2002)

35. M. Günther, A. Klar, T. Materne, R. Wegener

Multivalued fundamental diagrams and stop and go waves for continuum traffic equations

In the present paper a kinetic model for vehicular traffic leading to multivalued fundamental diagrams is developed and investigated in detail. For this model phase transitions can appear depending on the local density and velocity of the flow. A derivation of associated macroscopic traffic equations from the kinetic equation is given. Moreover, numerical experiments show the appearance of stop and go waves for highway traffic with a bottleneck.
Keywords: traffic flow, macroscopic equations, kinetic derivation, multivalued fundamental diagram, stop and go waves, phase transitions
(25 pages, 2002)

36. S. Feldmann, P. Lang, D. Prätzel-Wolters

Parameter influence on the zeros of network determinants

To a network N(q) with determinant D(s;q) depending on a parameter vector $q \hat{I} R^r$ via identification of some of its vertices, a network N^ (q) is assigned. The paper deals with procedures to find N^ (q), such that its determinant D^ (s;q) admits a factorization in the determinants of appropriate subnetworks, and with the estimation of the deviation of the zeros of D^ from the zeros of D. To solve the estimation problem state space methods are applied.
Keywords: Networks, Equicofactor matrix polynomials, Realization theory, Matrix perturbation theory
(30 pages, 2002)

37. K. Koch, J. Ohser, K. Schladitz

Spectral theory for random closed sets and estimating the covariance via frequency space

A spectral theory for stationary random closed sets is developed and provided with a sound mathematical basis. Definition and proof of existence of the Bartlett spectrum of a stationary random closed set as well as the proof of a Wiener-Khintchine theorem for the power spectrum are used to two ends: First, well known second order characteristics like the covariance can be estimated faster than usual via frequency space. Second, the Bartlett spectrum and the power spectrum can be used as second order characteristics in frequency space. Examples show, that in some cases information about the random closed set is easier to obtain from these characteristics in frequency space than from their real world counterparts.
Keywords: Random set, Bartlett spectrum, fast Fourier transform, power spectrum
(28 pages, 2002)

38. D. d'Humières, I. Ginzburg

Multi-reflection boundary conditions for lattice Boltzmann models

We present a unified approach of several boundary conditions for lattice Boltzmann models. Its general framework is a generalization of previously introduced schemes such as the bounce-back rule, linear or quadratic interpolations, etc. The objectives are two fold: first to give theoretical tools to study the existing boundary conditions and their corresponding accuracy; secondly to design formally third- order accurate boundary conditions for general flows. Using these boundary conditions, Couette and Poiseuille flows are exact solution of the lattice Boltzmann models for a Reynolds number $Re = 0$ (Stokes limit).
Numerical comparisons are given for Stokes flows in periodic arrays of spheres and cylinders, linear periodic array of cylinders between moving plates and for Navier-Stokes flows in periodic arrays of cylinders for $Re < 200$. These results show a significant improvement of the overall accuracy when using the linear interpolations instead of the bounce-back reflection (up to an order of magnitude on the hydrodynamics fields). Further improvement is achieved with the new multi-reflection boundary conditions, reaching a level of accuracy close to the quasi-analytical reference solutions, even for rather modest grid resolutions and few points in the narrowest channels. More important, the pressure and velocity fields in the vicinity of the obstacles are much smoother with multi-reflection than with the other boundary conditions.
Finally the good stability of these schemes is highlighted by some simulations of moving obstacles: a cylinder between flat walls and a sphere in a cylinder.
Keywords: lattice Boltzmann equation, boudary condistions, bounce-back rule, Navier-Stokes equation
(72 pages, 2002)

39. R. Korn

Elementare Finanzmathematik

Im Rahmen dieser Arbeit soll eine elementar gehaltene Einführung in die Aufgabenstellungen und Prinzipien der modernen Finanzmathematik gegeben werden. Insbesondere werden die Grundlagen der Modellierung von Aktienkursen, der Bewertung von Optionen und der Portfolio-Optimierung vorgestellt. Natürlich können die verwendeten Methoden und die entwickelte Theorie nicht in voller Allgemeinheit für den Schulunterricht verwendet werden, doch sollen einzelne Prinzipien so heraus gearbeitet werden, dass sie auch an einfachen Beispielen verstanden werden können.
Keywords: Finanzmathematik, Aktien, Optionen, Portfolio-Optimierung, Börse, Lehrerweiterbildung, Mathematikunterricht
(98 pages, 2002)

40. J. Kallrath, M. C. Müller, S. Nickel

Batch Presorting Problems: Models and Complexity Results

In this paper we consider short term storage systems. We analyze presorting strategies to improve the effiency of these storage systems. The presorting task is called Batch PreSorting Problem (BPSP). The BPSP is a variation of an assigment problem, i. e., it has an assigment problem kernel and some additional constraints. We present different types of these presorting problems, introduce mathematical programming formulations and prove the NP-completeness for one type of the BPSP. Experiments are carried out in order to compare the different model formulations and to investigate the behavior of these models.
Keywords: Complexity theory, Integer programming, Assigment, Logistics
(19 pages, 2002)

41. J. Linn

On the frame-invariant description of the phase space of the Folgar-Tucker equation

The Folgar-Tucker equation is used in flow simulations of fiber suspensions to predict fiber orientation depending on the local flow. In this paper, a complete, frame-invariant description of the phase space of this differential equation is presented for the first time.
Key words: fiber orientation, Folgar-Tucker equation, injection molding
(5 pages, 2003)

42. T. Hanne, S. Nickel

A Multi-Objective Evolutionary Algorithm for Scheduling and Inspection Planning in Software Development Projects

In this article, we consider the problem of planning inspections and other tasks within a software development (SD) project with respect to the objectives quality (no. of defects), project duration, and costs. Based on a discrete-event simulation model of SD processes comprising the phases coding, inspection, test, and rework, we present a simplified formulation of the problem as a multiobjective optimization problem. For solving the problem (i. e. finding an approximation of the efficient set) we develop a multiobjective evolutionary algorithm. Details of the algorithm are discussed as well as results of its application to sample problems.
Key words: multiple objective programming, project management and scheduling, software development, evolutionary algorithms, efficient set
(29 pages, 2003)

43. T. Bortfeld , K.-H. Küfer, M. Monz, A. Scherrer, C. Thieke, H. Trinkaus

Intensity-Modulated Radiotherapy - A Large Scale Multi-Criteria Programming Problem -

Radiation therapy planning is always a tight rope walk between dangerous insufficient dose in the target volume and life threatening overdosing of organs at risk. Finding ideal balances between these inherently contradictory goals challenges dosimetrists and physicians in their daily practice. Today's planning systems are typically based on a single evaluation function that measures the quality of a radiation treatment plan. Unfortunately, such a one dimensional approach can-

not satisfactorily map the different backgrounds of physicians and the patient dependent necessities. So, too often a time consuming iteration process between evaluation of dose distribution and redefinition of the evaluation function is needed.
In this paper we propose a generic multi-criteria approach based on Pareto's solution concept. For each entity of interest - target volume or organ at risk a structure dependent evaluation function is defined measuring deviations from ideal doses that are calculated from statistical functions. A reasonable bunch of clinically meaningful Pareto optimal solutions are stored in a data base, which can be interactively searched by physicians. The system guarantees dynamical planning as well as the discussion of tradeoffs between different entities.
Mathematically, we model the upcoming inverse problem as a multi-criteria linear programming problem. Because of the large scale nature of the problem it is not possible to solve the problem in a 3D-setting without adaptive reduction by appropriate approximation schemes.
Our approach is twofold: First, the discretization of the continuous problem is based on an adaptive hierarchical clustering process which is used for a local refinement of constraints during the optimization procedure. Second, the set of Pareto optimal solutions is approximated by an adaptive grid of representatives that are found by a hybrid process of calculating extreme compromises and interpolation methods.
Keywords: multiple criteria optimization, representative systems of Pareto solutions, adaptive triangulation, clustering and disaggregation techniques, visualization of Pareto solutions, medical physics, external beam radiotherapy planning, intensity modulated radiotherapy
(31 pages, 2003)

44. T. Halfmann, T. Wichmann

Overview of Symbolic Methods in Industrial Analog Circuit Design

Industrial analog circuits are usually designed using numerical simulation tools. To obtain a deeper circuit understanding, symbolic analysis techniques can additionally be applied. Approximation methods which reduce the complexity of symbolic expressions are needed in order to handle industrial-sized problems. This paper will give an overview to the field of symbolic analog circuit analysis. Starting with a motivation, the state-of-the-art simplification algorithms for linear as well as for nonlinear circuits are presented. The basic ideas behind the different techniques are described, whereas the technical details can be found in the cited references. Finally, the application of linear and nonlinear symbolic analysis will be shown on two example circuits.
Keywords: CAD, automated analog circuit design, symbolic analysis, computer algebra, behavioral modeling, system simulation, circuit sizing, macro modeling, differential-algebraic equations, index
(17 pages, 2003)

45. S. E. Mikhailov, J. Orlik

Asymptotic Homogenisation in Strength and Fatigue Durability Analysis of Composites

Asymptotic homogenisation technique and two-scale convergence is used for analysis of macro-strength and fatigue durability of composites with a periodic structure under cyclic loading. The linear damage accumulation rule is employed in the phenomenological micro-durability conditions (for each component of the composite) under varying cyclic loading. Both local and non-local strength and durability conditions are analysed. The strong convergence of the strength and fatigue damage measure as the structure period tends to zero is proved and their limiting values are estimated.
Keywords: multiscale structures, asymptotic homogenization, strength, fatigue, singularity, non-local conditions
(14 pages, 2003)

46. P. Domínguez-Marín, P. Hansen, N. Mladenović, S. Nickel

Heuristic Procedures for Solving the Discrete Ordered Median Problem

We present two heuristic methods for solving the Discrete Ordered Median Problem (DOMP), for which no such approaches have been developed so far. The DOMP generalizes classical discrete facility location problems, such as the p-median, p-center and Uncapacitated Facility Location problems. The first procedure proposed in this paper is based on a genetic algorithm developed by Moreno Vega [MV96] for p-median and p-center problems. Additionally, a second heuristic approach based on the Variable Neighborhood Search metaheuristic (VNS) proposed by Hansen & Mladenovic [HM97] for the p-median problem is described. An extensive numerical study is presented to show the efficiency of both heuristics and compare them.
Keywords: genetic algorithms, variable neighborhood search, discrete facility location
(31 pages, 2003)

47. N. Boland, P. Domínguez-Marín, S. Nickel, J. Puerto

Exact Procedures for Solving the Discrete Ordered Median Problem

The Discrete Ordered Median Problem (DOMP) generalizes classical discrete location problems, such as the N-median, N-center and Uncapacitated Facility Location problems. It was introduced by Nickel [16], who formulated it as both a nonlinear and a linear integer program. We propose an alternative integer linear programming formulation for the DOMP, discuss relationships between both integer linear programming formulations, and show how properties of optimal solutions can be used to strengthen these formulations. Moreover, we present a specific branch and bound procedure to solve the DOMP more efficiently. We test the integer linear programming formulations and this branch and bound method computationally on randomly generated test problems.
Keywords: discrete location, Integer programming
(41 pages, 2003)

48. S. Feldmann, P. Lang

Padé-like reduction of stable discrete linear systems preserving their stability

A new stability preserving model reduction algorithm for discrete linear SISO-systems based on their impulse response is proposed. Similar to the Padé approximation, an equation system for the Markov parameters involving the Hankel matrix is considered, that here however is chosen to be of very high dimension. Although this equation system therefore in general cannot be solved exactly, it is proved that the approximate solution, computed via the Moore-Penrose inverse, gives rise to a stability preserving reduction scheme, a property that cannot be guaranteed for the Padé approach. Furthermore, the proposed algorithm is compared to another stability preserving reduction approach, namely the balanced truncation method, showing comparable performance of the reduced systems. The balanced truncation method however starts from a state space description of the systems and in general is expected to be more computational demanding.
Keywords: Discrete linear systems, model reduction, stability, Hankel matrix, Stein equation
(16 pages, 2003)

49. J. Kallrath, S. Nickel

A Polynomial Case of the Batch Presorting Problem

This paper presents new theoretical results for a special case of the batch presorting problem (BPSP). We will show tht this case can be solved in polynomial time. Offline and online algorithms are presented for solving the BPSP. Competetive analysis is used for comparing the algorithms.
Keywords: batch presorting problem, online optimization, competetive analysis, polynomial algorithms, logistics
(17 pages, 2003)

50. T. Hanne, H. L. Trinkaus

knowCube for MCDM – Visual and Interactive Support for Multicriteria Decision Making

In this paper, we present a novel multicriteria decision support system (MCDSS), called knowCube, consisting of components for knowledge organization, generation, and navigation. Knowledge organization rests upon a database for managing qualitative and quantitative criteria, together with add-on information. Knowledge generation serves filling the database via e. g. identification, optimization, classification or simulation. For "finding needles in haycocks", the knowledge navigation component supports graphical database retrieval and interactive, goal-oriented problem solving. Navigation "helpers" are, for instance, cascading criteria aggregations, modifiable metrics, ergonomic interfaces, and customizable visualizations. Examples from real-life projects, e.g. in industrial engineering and in the life sciences, illustrate the application of our MCDSS.
Key words: Multicriteria decision making, knowledge management, decision support systems, visual interfaces, interactive navigation, real-life applications.
(26 pages, 2003)

51. O. Iliev, V. Laptev

On Numerical Simulation of Flow Through Oil Filters

This paper concerns numerical simulation of flow through oil filters. Oil filters consist of filter housing (filter box), and a porous filtering medium, which completely separates the inlet from the outlet. We discuss mathematical models, describing coupled flows in the pure liquid subregions and in the porous filter media, as well as interface conditions between them. Further, we reformulate the problem in fictitious regions method manner, and discuss peculiarities of the numerical algorithm in solving the coupled system. Next, we show numerical results, validating the model and the

algorithm. Finally, we present results from simulation of 3-D oil flow through a real car filter.
Keywords: oil filters, coupled flow in plain and porous media, Navier-Stokes, Brinkman, numerical simulation
(8 pages, 2003)

52. W. Dörfler, O. Iliev, D. Stoyanov, D. Vassileva

On a Multigrid Adaptive Refinement Solver for Saturated Non-Newtonian Flow in Porous Media

A multigrid adaptive refinement algorithm for non-Newtonian flow in porous media is presented. The saturated flow of a non-Newtonian fluid is described by the continuity equation and the generalized Darcy law. The resulting second order nonlinear elliptic equation is discretized by a finite volume method on a cell-centered grid. A nonlinear full-multigrid, full-approximation-storage algorithm is implemented. As a smoother, a single grid solver based on Picard linearization and Gauss-Seidel relaxation is used. Further, a local refinement multigrid algorithm on a composite grid is developed. A residual based error indicator is used in the adaptive refinement criterion. A special implementation approach is used, which allows us to perform unstructured local refinement in conjunction with the finite volume discretization. Several results from numerical experiments are presented in order to examine the performance of the solver.
Keywords: Nonlinear multigrid, adaptive refinement, non-Newtonian flow in porous media
(17 pages, 2003)

53. S. Kruse

On the Pricing of Forward Starting Options under Stochastic Volatility

We consider the problem of pricing European forward starting options in the presence of stochastic volatility. By performing a change of measure using the asset price at the time of strike determination as a numeraire, we derive a closed-form solution based on Heston's model of stochastic volatility.
Keywords: Option pricing, forward starting options, Heston model, stochastic volatility, cliquet options
(11 pages, 2003)

54. O. Iliev, D. Stoyanov

Multigrid – adaptive local refinement solver for incompressible flows

A non-linear multigrid solver for incompressible Navier-Stokes equations, exploiting finite volume discretization of the equations, is extended by adaptive local refinement. The multigrid is the outer iterative cycle, while the SIMPLE algorithm is used as a smoothing procedure. Error indicators are used to define the refinement subdomain. A special implementation approach is used, which allows to perform unstructured local refinement in conjunction with the finite volume discretization. The multigrid - adaptive local refinement algorithm is tested on 2D Poisson equation and further is applied to a lid-driven flows in a cavity (2D and 3D case), comparing the results with bench-mark data. The software design principles of the solver are also discussed.
Keywords: Navier-Stokes equations, incompressible flow, projection-type splitting, SIMPLE, multigrid methods, adaptive local refinement, lid-driven flow in a cavity
(37 pages, 2003)

55. V. Starikovicius

The multiphase flow and heat transfer in porous media

In first part of this work, summaries of traditional Multiphase Flow Model and more recent Multiphase Mixture Model are presented. Attention is being paid to attempts include various heterogeneous aspects into models. In second part, MMM based differential model for two-phase immiscible flow in porous media is considered. A numerical scheme based on the sequential solution procedure and control volume based finite difference schemes for the pressure and saturation-conservation equations is developed. A computer simulator is built, which exploits object-oriented programming techniques. Numerical result for several test problems are reported.
Keywords: Two-phase flow in porous media, various formulations, global pressure, multiphase mixture model, numerical simulation
(30 pages, 2003)

56. P. Lang, A. Sarishvili, A. Wirsen

Blocked neural networks for knowledge extraction in the software development process

One of the main goals of an organization developing software is to increase the quality of the software while at the same time to decrease the costs and the duration of the development process. To achieve this, various decisions e.ecting this goal before and during the development process have to be made by the managers. One appropriate tool for decision support are simulation models of the software life cycle, which also help to understand the dynamics of the software development process. Building up a simulation model requires a mathematical description of the interactions between di.erent objects involved in the development process. Based on experimental data, techniques from the .eld of knowledge discovery can be used to quantify these interactions and to generate new process knowledge based on the analysis of the determined relationships. In this paper blocked neuronal networks and related relevance measures will be presented as an appropriate tool for quanti.cation and validation of qualitatively known dependencies in the software development process.
Keywords: Blocked Neural Networks, Nonlinear Regression, Knowledge Extraction, Code Inspection
(21 pages, 2003)

57. H. Knaf, P. Lang, S. Zeiser

Diagnosis aiding in Regulation Thermography using Fuzzy Logic

The objective of the present article is to give an overview of an application of Fuzzy Logic in Regulation Thermography, a method of medical diagnosis support. An introduction to this method of the complementary medical science based on temperature measurements – so-called thermograms – is provided. The process of modelling the physician's thermogram evaluation rules using the calculus of Fuzzy Logic is explained.
Keywords: fuzzy logic,knowledge representation, expert system
(22 pages, 2003)

58. M.T. Melo, S. Nickel, F. Saldanha da Gama

Largescale models for dynamic multi-commodity capacitated facility location

In this paper we focus on the strategic design of supply chain networks. We propose a mathematical modeling framework that captures many practical aspects of network design problems simultaneously but which have not received adequate attention in the literature. The aspects considered include: dynamic planning horizon, generic supply chain network structure, external supply of materials, inventory opportunities for goods, distribution of commodities, facility configuration, availability of capital for investments, and storage limitations. Moreover, network configuration decisions concerning the gradual relocation of facilities over the planning horizon are considered. To cope with fluctuating demands, capacity expansion and reduction scenarios are also analyzed as well as modular capacity shifts. The relation of the proposed modeling framework with existing models is discussed. For problems of reasonable size we report on our computational experience with standard mathematical programming software. In particular, useful insights on the impact of various factors on network design decisions are provided.
Keywords: supply chain management, strategic planning, dynamic location, modeling
(40 pages, 2003)

59. J. Orlik

Homogenization for contact problems with periodically rough surfaces

We consider the contact of two elastic bodies with rough surfaces at the interface. The size of the micro-peaks and valleys is very small compared with the macrosize of the bodies' domains. This makes the direct application of the FEM for the calculation of the contact problem prohibitively costly. A method is developed that allows deriving a macrocontact condition on the interface. The method involves the twoscale asymptotic homogenization procedure that takes into account the microgeometry of the interface layer and the stiffnesses of materials of both domains. The macrocontact condition can then be used in a FEM model for the contact problem on the macrolevel. The averaged contact stiffness obtained allows the replacement of the interface layer in the macromodel by the macrocontact condition.
Keywords: asymptotic homogenization, contact problems
(28 pages, 2004)

Status quo: January 2004